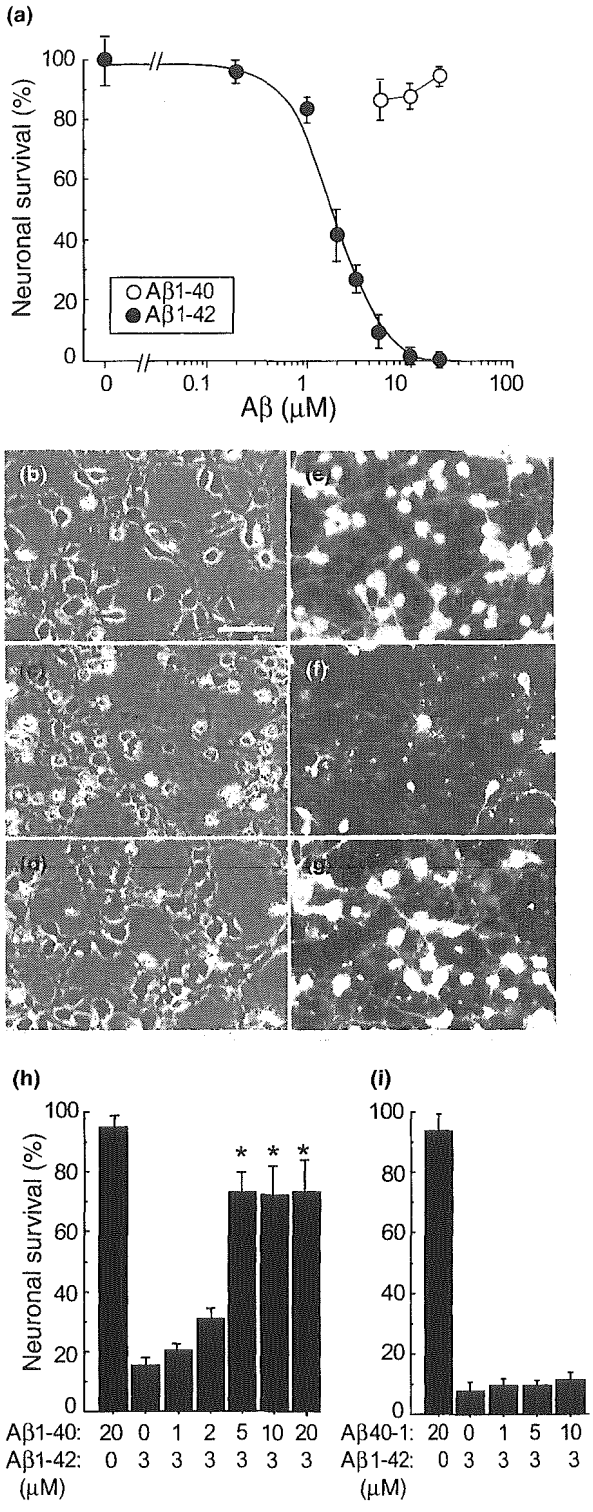

Fig. 1 Aβ1–40 prevents the neuronal death induced by Aβ1–42. Rat embryonic cortical neurons were cultured in N2 medium. Twenty-four hours after plating, neurons were treated with freshly dissolved Aβ1–42 or Aβ1–40 at various concentrations. Cell viability in each culture was determined 48 h after the commencement of the treatment (a). Twenty-four hours after plating, 3 or 4 μm Aβ1–42 was added to neuronal cultures maintained in N2 medium with or without the pre-treatment (1 h before the addition of Aβ1–42) with Aβ1–40 at various concentrations. Forty-eight hours after the commencement of the treatment, the photomicrographs of each culture were taken with (e–g) or without (b–d) calcein AM staining to determine neuronal survival. (b, e) Control treatment with DMSO vehicle; (c, f) 4 μM Aβ1–42; (d, g) 4 μM Aβ1–42 and 20 μM Aβ1–40; (h) neuronal survival in cultures treated with Aβ1–42 plus Aβ1–40 at various concentrations; (i) neuronal survival in cultures treated with Aβ1–42 plus Aβ40–1 at various concentrations.

demonstrated by phase-contrast photomicrography and calcein AM staining (Fig. 1a), while treatment with 5–20 μM Aβ1–40 alone did not affect the neuronal survival (Fig. 1a). When neurons were treated with freshly prepared 4 μM Aβ1–42, most of the cultured neurons died 48 h after the commencement of the treatment (Figs 1c and f). Surprisingly, neuronal death was prevented in the presence of 20 μM Aβ1–40 (Figs 1d and g). Neuronal death induced by Aβ1–42 was prevented by Aβ1–40 in a dose-dependent manner. Two micromolar Aβ1–40 partially protected neurons against the neurotoxicity induced by 3 μM Aβ1–42, and Aβ1–40 at concentration higher than 5 μM afforded the full protective effect (Fig. 1h). However, Aβ40–1 could not ameliorate the Aβ1–42 toxicity (Fig. 1i). The neuroprotective effect of Aβ1–40 may be incomplete, because some neurons treated with Aβ1–42 plus Aβ1–40 showed dystrophy with less neuronal network compared with the non-treated neurons; however, neuronal death induced by Aβ1–42 was effectively prevented (Figs 1b–g and h).

Metal chelators have no effect on neurotoxicity of Aβ1–42

We have found that Aβ1–40 has antioxidant activity against metal-induced oxidative damage by binding and sequestrating transition metal ions (Zou *et al.* 2002). Previous reports suggest that Aβ1–42 toxicity is due to the interaction of Aβ1–42 with the transition metals, resulting in the generation of neurotoxic H_2O_2 (Opazo *et al.* 2002) and the disruption of membrane structure (Curtain *et al.* 2001). Thus, we examined whether the depletion of metals by metal chelators can ameliorate the Aβ1–42 toxicity. Primary cultured neurons were treated with 2 μM Aβ1–42 with or without the pre-treatment with 10 μM Aβ1–40, 400 μM EDTA, 40 μM CDTA or 8 μM DTPA. Aβ1–40 protected neurons, whereas EDTA, CDTA and DTPA, which rescued neurons from iron-dependent oxidative stress (Zou *et al.* 2002), did not protect neurons against Aβ1–42-induced death (Table 1). These results indicate that the neuroprotective action of Aβ1–40 against the Aβ1–42-induced neurotoxicity is independent of its metal-binding capability and that the Aβ1–42 toxicity, at least in part, is not dependent on the presence of metal ions in the culture medium.

Table 1 Metal chelators have no effect on the neurotoxicity of Aβ1–42

Aβ1–42 (2 μM)	Concentration	Neuronal survival (% of non-treated cultures)
Control	–	36 ± 6
Aβ1–40	10 μM	78 ± 5[a]
EDTA	400 μM	40 ± 1
CDTA	40 μM	33 ± 6
DTPA	8 μM	31 ± 5

Cortical neurons were prepared from brains of rat embryo and cultured in N2 medium as described in Materials and methods. Twenty-four hours after plating, 2 μM Aβ1–42 was added to neuronal cultures maintained in N2 medium with or without the pre-treatment (1 h before the addition of Aβ1–42) with Aβ1–40, EDTA, CDTA or DTPA. The cultures were maintained for another 48 h and then the neuronal survival was determined. Each value represents the mean ± SE of four samples. [a]$p < 0.001$ versus control.

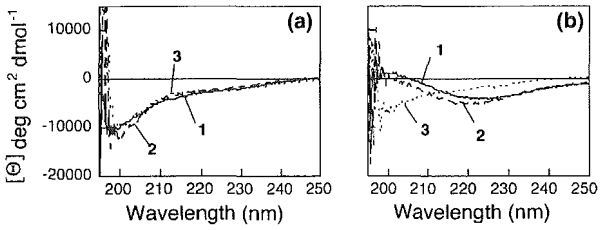

Fig. 2 Inhibitory effect of Aβ1–40 on β-sheet transformation of Aβ1–42. CD spectra of 10 μM Aβ1–42, 40 μM Aβ1–16, 20 μM Aβ1–40, a mixture of 10 μM Aβ1–42 and 40 μM Aβ1–16, and a mixture of 10 μM Aβ1–42 and 20 μM Aβ1–40 in PBS were measured as a function of incubation time at 37°C. Spectra originating from Aβ1–42 at 0 h (a) and after 4 h of incubation (b) were estimated by subtracting the spectra of Aβ1–16 or Aβ1–40 alone from those of the physical mixtures. Trace 1, Aβ1–42 alone; trace 2, Aβ1–42 + Aβ1–16; Aβ1–42 + Aβ1–40.

Freshly prepared Aβ 1–40 inhibits β-sheet transformation of Aβ1–42

Because the secondary structure of Aβ is known to correlate with neurotoxic activity *in vitro* (Simmons *et al.* 1994), we then examined the β-sheet transformation of Aβ1–42 alone and Aβ1–42 mixed with Aβ1–40 or a short Aβ peptide, Aβ1–16. Figure 2 shows CD spectra for Aβ1–42 alone (trace 1), Aβ1–42 with Aβ1–16 (trace 2), and Aβ1–42 with Aβ1–40 (trace 3) incubated at 37°C. Spectral contributions from Aβ1–16 or Aβ1–40 were corrected by subtracting the spectra of Aβ1–16 or Aβ1–40 alone, which are characterized by having random structures, from the spectra of the physical mixtures. Freshly dissolved peptides showed spectra with minima around 197 nm, which indicate the predominance of unordered structures (Fig. 2a). There was no interaction between the different peptides, because all spectra were superimposable. After a 4-h incubation (Fig. 2b), the spectrum of Aβ1–42 alone exhibited a minimum around 225 nm and became positive below 206 nm, indicating a conformational change to a β-structure (trace 1). The co-existence of Aβ1–16 and Aβ1–42 could not inhibit the β-sheet formation (trace 2). In contrast, the presence of Aβ1–40 inhibited structural transition (trace 3): Aβ1–42 remained a random structure. Because this experiment was perform in PBS(–), which is metal-ion-free, these results indicate that Aβ1–40 protects neurons against Aβ1–42-induced neurotoxicity by retaining Aβ1–42 as a random structure and probably not by inhibiting transition metal-dependent oxygen radical generation.

Freshly prepared Aβ1–40 inhibits fibril formation of Aβ1–42 both in DMEM/F12 medium and in PBS(–)

Four micromolar Aβ1–42 was incubated in the DMEM/F12 medium at 37°C overnight with or without Aβ1–40, Aβ1–16, Aβ25–35, or Aβ40–1. Aβ1–40 dose-dependently decreased the thioflavin-T fluorescence value, indicating that the aggregation of Aβ1–42 was inhibited, whereas short Aβ peptides, Aβ1–16 and Aβ25–35, and reversed peptides, Aβ40–1, had no effect (Fig. 3a). We also examined the fibril formation by electron microscopy. Ten micromolar Aβ1–42 was incubated at 37°C overnight with or without 20 μM Aβ1–40, 40 μM Aβ1–16 or 40 μM Aβ25–35. Fibrils were formed by Aβ1–42 alone, Aβ1–42 with Aβ1–16, and Aβ1–42 with Aβ25–35. In contrast, Aβ1–42 with Aβ1–40 failed to form fibrils, only a small amount of protofibrils could be observed (Fig. 3b). Aβ1–40 inhibited the fibril formation of Aβ1–42 in PBS(–), indicating that the inhibitory action of Aβ1–40 against the fibril formation of Aβ1–42 is metal-independent.

Short Aβ peptides have no inhibitory action against Aβ1–42-induced neurotoxicity

We examined the neuroprotective action of Aβ1–16 and Aβ25–35, in addition to Aβ1–40, against the neurotoxicity induced by Aβ1–42. Aβ1–40, Aβ1–16 or Aβ25–35 was added to the culture medium and the cultured neurons were then treated with 3 μM Aβ1–42. As we expected, among the peptides examined, only Aβ1–40 significantly prevented neuronal death induced by Aβ1–42 (Fig. 3c). Aβ1–16 or Aβ25–35 neither prevented nor promoted neuronal death. These results indicate that the ability to inhibit the β-sheet transformation and fibril formation of Aβ1–42 is necessary for the protection of neurons.

Aβ1–42 stimulates tau phosphorylation and activates astrocytes, which are inhibited by concurrent treatment with Aβ1–40 in rat brain

To evaluate the inhibitory action of Aβ1–40 against Aβ1–42-induced neuronal damage *in vivo*, we have established a rat model system in order to observe the phosphorylation state of tau and activation of astrocytes by injecting freshly solubilized Aβ1–42 directly into the entorhinal cortex (EC).

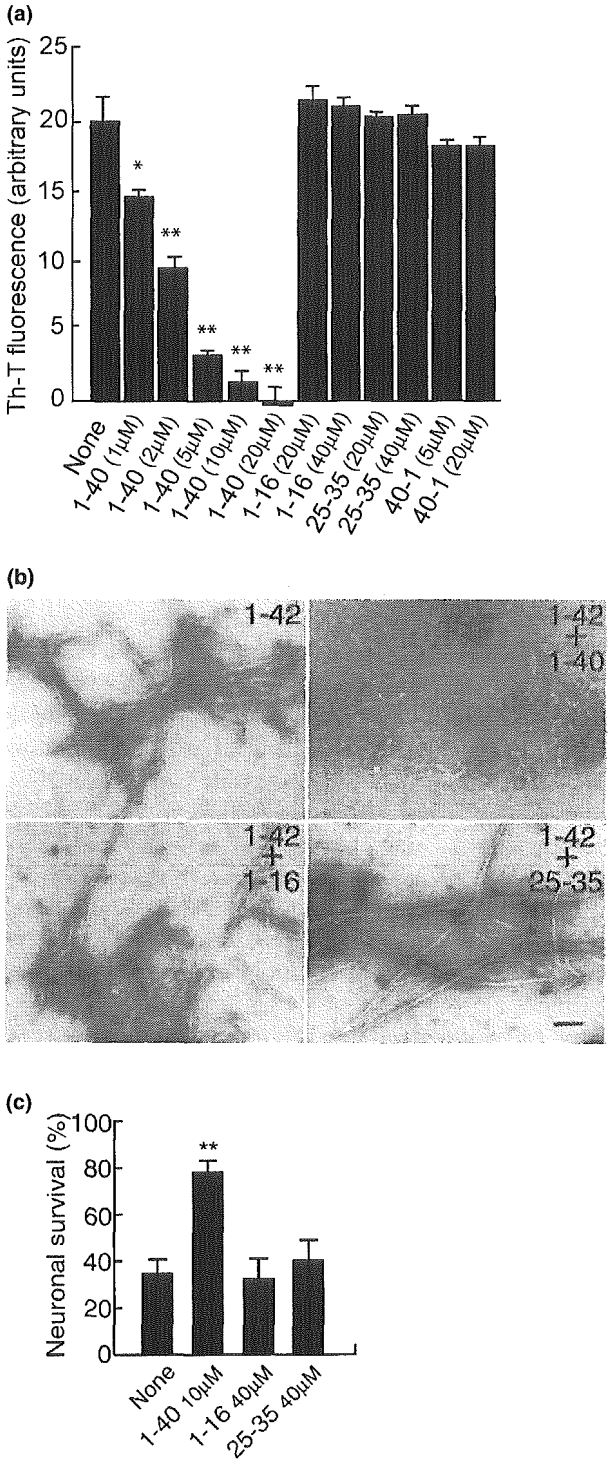

Fig. 3 Aβ1–40 inhibits the fibril formation of Aβ1–42. (a) One millilitre of 4 μM Aβ1–42 was incubated in DMEM/F12 at 37°C for 24 h with or without Aβ1–40, Aβ1–16, Aβ25–35 or Aβ40–1 at various concentrations. The samples were centrifuged and the thioflavin-T fluorescence intensity of precipitates was determined. (b) One millilitre of 10 μM Aβ1–42 was incubated in PBS(–) at 37°C for 24 h with or without 20 μM Aβ1–40, 40 μM Aβ1–16 or 40 μM Aβ25–35. The samples were centrifuged and the morphology of fibrils recovered from the bottom part of the supernatant (50 μL) was analyzed under a transmission electron microscope. (c) Ten micromolars Aβ1–40, 40 μM Aβ1–16 or 40 μM Aβ25–35 was added to neuronal cultures in the N2 medium 24 h after plating, followed by the addition of 3 μM Aβ1–42. The cultures were then incubated for another 48 h and the neuronal survival was determined. Three independent experiments showed similar results. Each value represents the mean ± SE of four samples. $^*p < 0.01$ $^{**}p < 0.01$ versus none, respectively.

All the rats injected with Aβ1–42, Aβ1–42 plus Aβ1–40, or PBS survived for 3 days after surgery. The rats were then anaesthetized. The EC and hippocampus were then removed for analysis. We applied various concentrations (0.001, 0.01, 0.1, 1, 10, 100, and 200 μM) of Aβ1–42 and the effect of those injections was determined. Consistent with a previous study (Soto *et al.* 1998), in the present study, Aβ1–42 at concentrations higher than 100 μM has biological effects on brain cells *in vivo*. Figures 4(a and b) show the representative results indicating that Aβ1–42 injection (200 μM, 5 μL) significantly promoted tau phosphorylation at multiple sites as demonstrated by immunoblot analysis using site-specific antiphospho-tau antibodies, AT-8, AT-100, and PHF-1. However, injection of 2.5 μL of Aβ1–42 (400 μM) plus 2.5 μL of Aβ1–40 (800 μM) or 5 μL of PBS(–) did not cause such phosphorylation (Figs 4a and b). Total tau protein levels were not altered among these samples as demonstrated by immunoblot analysis using the antiphospho-independent tau antibody, T46 (Figs 4a and b). Aβ1–42 injection into the EC also promoted tau phosphorylation at multiple sites in the hippocampus of the injected side, while Aβ1–42 plus Aβ1–40 or PBS injection did not (Figs 4c and d), indicating a remote effect of Aβ1–42 injection. We next determined the effect of Aβ peptide injection on the induction of reactive astrocytes in rat brains. As shown in Fig. 5 and Table 2, Aβ1–42 injection increased the number of GFAP-positive astrocytes in the surrounding regions of the injection scar, while Aβ1–42 plus Aβ1–40 or PBS injection did not. We also performed Congo red staining of these samples and found that Aβ1–42 (100 μM) injected into EC formed Congo red-positive structure, amyloid, in the injected site, while coinjection with Aβ1–40 prevented it (data not shown).

Discussion

We show that Aβ1–40 serves as a natural inhibitor of Aβ1–42-induced neurotoxicity by inhibiting β-sheet transformation of Aβ1–42. In *in vivo* experiments, Aβ1–40 also prevented cell damage induced by Aβ1–42. Aβ is widely believed to serve as a neurotoxic molecule generating oxygen radicals by its interaction with redox-active metal ions, which

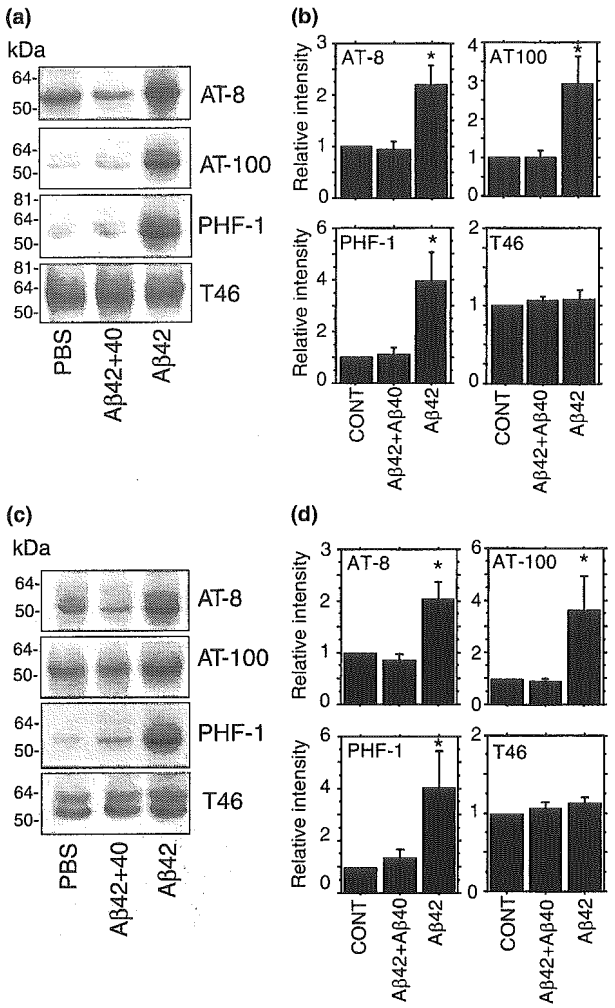

Fig. 4 Western blot analysis of tau in the injected sites of EC and hippocampus. Mice were anaesthetized and reagents including 5 μL of PBS, 5 μL of Aβ1–42 (200 μM), or 2.5 μL of Aβ1–42 (400 μM) + 2.5 μL of Aβ1–40 (800 μM) were injected into the EC. The animals were allowed to survive for 3 days, and then the EC and hippocampus were removed from these rats as described in Materials and methods. Equivalent amounts of postnuclear supernatant protein from the injected sites of EC (a) and hippocampus (b) were separated using 10% sodium SDS–PAGE. Separated proteins were transferred onto PVDF membranes and probed with the site-specific antiphospho-tau antibodies, AT-8, AT-100, and PHF-1 in addition to phospho-independent anti-tau antibody, T46. The intensity of each immunoreactive signal for these antibodies was analyzed using an NIH image analyzer (Macintosh). The intensity ratios for each sample/control of EC (c) and hippocampus (d) are shown. Each value is the mean ± SE of triplicates. *$p < 0.05$ versus CONT and Aβ1–40 + Aβ1–42.

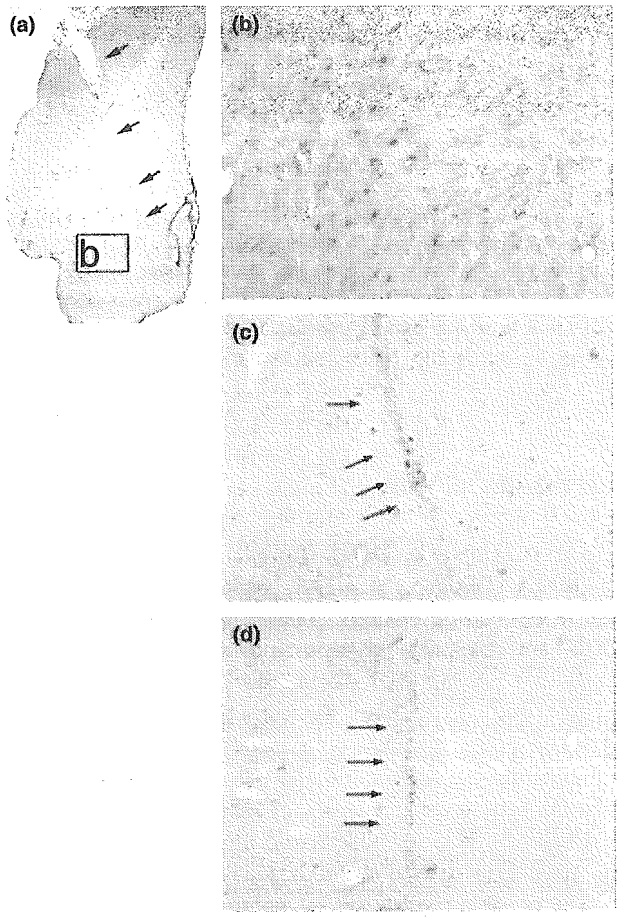

Fig. 5 Immunohistochemistry of the injected EC sites using anti-GFAP antibody. Three days after the injections of 5 μL of PBS, 5 μL of Aβ1–42 (200 μM), or 2.5 μL of Aβ1–42 (400 μM) + 2.5 μL of Aβ1–40 (800 μM) into the EC, the animals were re-anaesthetized and their brains were removed and fixed to prepare tissue sections from the injected EC sites as described in Materials and methods. The tissue sections were incubated overnight at 4°C with the monoclonal anti-GFAP antibody (Chemicon, Temecura, CA, USA, 1 : 100) in 0.1 M sodium phosphate buffer containing 1% normal donkey serum and 0.3% Triton X-100. The sections were then incubated with biotinylated goat anti-mouse IgG, rinsed in PBS, incubated in the avidin-biotin complex solution, and visualized with a solution of 0.003% H_2O_2 and 0.05% 3,3′-diaminobenzidine in 0.1 M PB. (a) EC site injected with Aβ1–42. Arrows indicate the injection scar (× 12.5). (b) Number of GFAP-positive cells that were observed near the injected site (× 200). The same area boxed as b in Fig. 5(a). In contrast, no GFAP-positive cells were found in the EC sites injected with Aβ1–42 plus Aβ1–40 (c) or PBS (d) (× 200). Arrows indicate the injection scars.

is suppressed by the redox-inactive form of zinc or metal ion chelators (Huang *et al.* 1999a,b; Cuajungco *et al.* 2000). In our previous study, however, we showed that monomeric Aβ1–40 can serve as an antioxidant molecule against metal-induced oxidative damage by sequestrating metal ions and inhibiting the redox reaction induced by transition metals (Zou *et al.* 2002). Metal ions, such as iron, copper and zinc, were shown to promote Aβ aggregation (Bush *et al.* 1994; Huang *et al.* 1997; Atwood *et al.* 1998), which is reversed by treatment with chelators *in vitro* (Huang *et al.* 1997) and

Table 2 Number of GFAP-positive cells in rat brains injected with Aβ1–42, Aβ1–42 + Aβ1–40 or PBS

	Number of GFAP-positive cells/cm^2		
Distance from the scar edge (μM)	Aβ1–42 (9 slides from 3 animals)	Aβ1–42 + Aβ1–40 (16 slides from 5 animals)	PBS (8 slides from 3 animals)
0–500	185.9 ± 12.1	0	0
500–1000	60.0 ± 5.3	0	0

Aβ1–42, Aβ1–42 + Aβ1–40 or PBS was injected into the EC of the rat brains. Three days following the injections, the brains were removed, fixed to prepare tissue sections, and immunostained using an anti-GFAP antibody as described in Materials and methods. In order to exclude the GFAP-positive cells arising from the injection itself, we counted the GFAP-positive cells in an area from the edge of the injection scar but not from the center of the injection scar. Thus, the GFAP-positive cells were counted in an area between 0 and 500 μM from the edge of the injection scar and in an area between 500 and 1000 μM from the edge of the injection scar. The GFAP-positive cell number per cm^2 was then calculated. Each value represents the mean number of GFAP-positive cells/cm^2 ± SEM for each treatment.

in vivo (Cherny *et al.* 2001). However, metal chelators, such as EDTA, CDTA, and DTPA, which effectively prevent metal ion-induced oxidative damage on neurons (Zou *et al.* 2002) and disrupt the aggregation of Aβ induced by metals, could not prevent Aβ1–42-induced neuronal death in the present study. In addition, we found that fibril formation of Aβ1–42 occurs in PBS(–), a metal-free buffer, which is inhibited by the addition of Aβ1–40. These results indicate that the neuroprotective action of Aβ1–40 against Aβ1–42-induced neurotoxicity observed in this study is unrelated to its metal sequestration or antioxidation ability.

The possible mechanism by which Aβ1–42 causes neuronal death may be related to the formation of Aβ oligomers and aggregates. Several lines of evidence show that oligomers or aggregates, both of which contain β-sheet-rich Aβ, are required for Aβ to exhibit neurotoxicity (Simmons *et al.* 1994). The suggested underlying mechanisms are as follows: oligomeric and aggregated Aβ can cause membrane dysfunction and damage (Avdulov *et al.* 1997; Kourie and Henry 2001; Yip *et al.* 2001). Our findings that Aβ1–42 rapidly aggregates and forms fibrils in PBS(–), which does not contain any metals (Fig. 3b), and that Aβ1–40 effectively inhibits β-sheet transformation and the subsequent fibril formation of Aβ1–42 in PBS(–) (Fig. 3b), support this notion. One may say that PBS(–) contains trace metals and they cause Aβ1–42 aggregation; however, metal chelators, EDTA, CDTA, DTPA, and EGTA, did not inhibit Aβ1–42 aggregation in PBS(–) (data not shown), suggesting that this is not the case. CD spectrum analysis clearly showed the mechanism underlying the inhibitory effect of Aβ1–40 on the β-sheet transformation of Aβ1–42: Aβ1–40 directly interacts with Aβ1–42 and inhibits the β-sheet transformation of Aβ1–42 (Fig. 2). The lack of such effects of Aβ1–16 suggests that Leu17–Val40 of Aβ1–40 is necessary for these interactions. Indeed, the hydrophobic core Leu17–Ala21 has been reported to be important for the formation of amyloid fibrils (Hilbich *et al.* 1992). This previous report partly supports our results that under *in vitro* conditions, 20 μM Aβ1–40 does not form amyloid, while Aβ1–42 immediately forms amyloid, and Aβ1–40 inhibits amyloid formation of Aβ1–42 (Hasegawa *et al.* 1999). However, we for the first time show the biological effect of Aβ1–40 on Aβ1–42-induced neuronal damage in culture and in rat brains.

We also found the protective action of Aβ1–40 against Aβ1–42-induced neuronal damage demonstrated as the promotion of tau phosphorylation and activation of astrocytes in *in vivo* rat brains. The Aβ1–42 injection into EC not only promoted tau phosphorylation in the injected sites of EC, but also in the hippocampus spatially separated from EC, which was prevented by the concurrent presence of Aβ1–40. The interesting point is that tau was similarly hyperphosphorylated, not only in the ipsilateral hippocampus, but also in the contralateral hippocampus (data not shown). Although the molecular mechanisms of this remote effect of Aβ1–42 injection into the cortex on tau phosphorylation in the hippocampus remain to be determined, as the previous report suggested (Gotz *et al.* 2001), damage to presynaptic terminals or axons projecting to the injected sites may retrogradely promote tau phosphorylation. Aβ1–40 also inhibits the activation of astrocytes induced by Aβ1–42 injected to EC, suggesting that as observed in cultured neurons, Aβ1–40 prevents Aβ1–42-induced neuronal damage in rat brains.

These findings suggest the importance of the ratio of Aβ1–42/Aβ1–40, because the neuroprotective action of Aβ1–40 against Aβ1–42-induced cell death and the inhibitory effect of Aβ1–40 on the fibril formation of Aβ1–42 are Aβ1–40-concentration-dependent, that is, Aβ1–42/Aβ1–40-ratio-dependent. This may also provide a hypothetical explanation of the molecular mechanism underlying the observation that Aβ1–42/Aβ1–40 ratio elevation is the major determinant for the development of familial AD. However, this may not be the case for the Swedish-type mutation of APP (APPsw), because the mutation markedly (six- to eightfold of that in controls) increases the total Aβ concentrations *in vitro*

(Citron *et al.* 1992; Cai *et al.* 1993) and *in vivo* (Hsiao *et al.* 1996), while it does not change the Aβ1–42/Aβ1–40 ratio (Scheuner *et al.* 1996; Yan *et al.* 1999). In the case of APPsw, it may be possible that high concentrations of Aβ1–40 and Aβ1–42 generated in the central nervous system may exceed the capacities of Aβ degradation (Iwata *et al.* 2001) or clearance (Holtzman *et al.* 1999), allowing Aβ1–40 and Aβ1–42 to remain for a longer time, which in turn may lead to self-aggregation, subsequent Aβ deposition, and exhibition of neurotoxicity. However, transgenic mice doubly expressing presenilin 1 mutation and APPsw have shown accelerated Aβ deposition and AD pathologies compared with those expressing only APPsw (Borchelt *et al.* 1997; Holcomb *et al.* 1998; Urbanc *et al.* 2002), suggesting the critical role of the Aβ1–42/Aβ1–40 ratio in the development of AD pathologies even in a mouse model with APPsw.

Our present data show that Aβ1–40 fully reverses the Aβ1–42-induced neurotoxicity and fibril formation of Aβ1–42 in an Aβ1–40-concentration-dependent manner with a stoichiometry of 1.6–2.5 : 1 between Aβ1–40 and Aβ1–42. It is known that, under normal conditions, the concentration of Aβ1–42 is about 10% of total Aβ and in the case of familial AD, this can be elevated to approximately 20% of total Aβ. These lines of evidence indicate that the concentrations of Aβ1–40 are 5- to 10-fold those of Aβ1–42 in all AD cases and that, based on our present findings, the concentrations of Aβ1–40 are sufficient to prevent Aβ1–42-induced pathogenesis. This may be because additional factors modulate the formation of Aβ oligomers and fibrils (Yanagisawa *et al.* 1995), which may attenuate the neuroprotective effect of Aβ1–40. Our observations in the present study provide new insight into the specie-dependent functions of Aβ, that is, the novel neuroprotective function of Aβ1–40, the major Aβ peptide, against Aβ1–42-induced neurotoxicity.

Acknowledgements

This work was supported by the Longevity Sciences Grant (H14-010) from the Ministry of Health, Labor and Welfare, and a grant from the Organization for Pharmaceutical Safety and Research of Japan.

References

Amtul Z., Lewis P. A., Piper S. *et al.* (2002) A presenilin 1 mutation associated with familial frontotemporal dementia inhibits gamma-secretase cleavage of APP and notch. *Neurobiol. Dis.* **9**, 269–273.

Atwood C. S., Moir R. D., Huang X., Scarpa R. C., Bacarra N. M., Romano D. M., Hartshorn M. A., Tanzi R. E. and Bush A. I. (1998) Dramatic aggregation of Alzheimer Aβ by Cu(II) is induced by conditions representing physiological acidosis. *J. Biol. Chem.* **273**, 12817–12826.

Avdulov N. A., Chochina S. V., Igbavboa U., Warden C. S., Vassiliev A. V. and Wood W. G. (1997) Lipid binding to amyloid beta-peptide aggregates: preferential binding of cholesterol as compared with phosphatidylcholine and fatty acids. *J. Neurochem.* **69**, 1746–1752.

Borchelt D. R., Thinakaran G., Eckman C. B. *et al.* (1996) Familial Alzheimer's disease-linked presenilin 1 variants elevate Aβ1–42/1–40 ratio *in vitro* and *in vivo*. *Neuron* **17**, 1005–1013.

Borchelt D. R., Ratovitski T., van Lare J., Lee M. K., Gonzales V., Jenkins N. A., Copeland N. G., Price D. L. and Sisodia S. S. (1997) Accelerated amyloid deposition in the brains of transgenic mice coexpressing mutant presenilin 1 and amyloid precursor proteins. *Neuron* **19**, 939–945.

Bottenstein J. E. and Sato G. H. (1979) Growth of a rat neuroblastoma cell line in serum-free supplemented medium. *Proc. Natl Acad. Sci. USA* **76**, 514–517.

Bush A. I., Pettingell W. H., Multhaup G., d Paradis M., Vonsattel J. P., Gusella J. F., Beyreuther K., Masters C. L. and Tanzi R. E. (1994) Rapid induction of Alzheimer Aβ amyloid formation by zinc. *Science* **265**, 1464–1467.

Cai X. D., Golde T. E. and Younkin S. G. (1993) Release of excess amyloid beta protein from a mutant amyloid β-protein precursor. *Science* **259**, 514–516.

Cherny R. A., Atwood C. S., Xilinas M. E. *et al.* (2001) Treatment with a copper-zinc chelator markedly and rapidly inhibits β-amyloid accumulation in Alzheimer's disease transgenic mice. *Neuron* **30**, 665–676.

Citron M., Oltersdorf T., Haass C., McConlogue L., Hung A. Y., Seubert P., Vigo-Pelfrey C., Lieberburg I. and Selkoe D. J. (1992) Mutation of the β-amyloid precursor protein in familial Alzheimer's disease increases beta-protein production. *Nature* **360**, 672–674.

Citron M., Westaway D., Xia W. *et al.* (1997) Mutant presenilins of Alzheimer's disease increase production of 42-residue amyloid β-protein in both transfected cells and transgenic mice. *Nat. Med.* **3**, 67–72.

Cuajungco M. P., Goldstein L. E., Nunomura A., Smith M. A., Lim J. T., Atwood C. S., Huang X., Farrag Y. W., Perry G. and Bush A. I. (2000) Evidence that the β-amyloid plaques of Alzheimer's disease represent the redox-silencing and entombment of Aβ by zinc. *J. Biol. Chem.* **275**, 19439–19442.

Curtain C. C., Ali F., Volitakis I., Cherny R. A., Norton R. S., Beyreuther K., Barrow C. J., Masters C. L., Bush A. I. and Barnham K. J. (2001) Alzheimer's disease amyloid-β binds copper and zinc to generate an allosterically ordered membrane-penetrating structure containing superoxide dismutase-like subunits. *J. Biol. Chem.* **276**, 20466–20473.

Dore S., Kar S. and Quirion R. (1997) Insulin-like growth factor I protects and rescues hippocampal neurons against β-amyloid- and human amylin-induced toxicity. *Proc. Natl Acad. Sci. USA* **94**, 4772–4777.

Eckman C. B., Mehta N. D., Crook R. *et al.* (1997) A new pathogenic mutation in the APP gene (I716V) increases the relative proportion of Aβ42 (43). *Hum. Mol. Genet.* **6**, 2087–2089.

Glenner G. G. and Wong C. W. (1984) Alzheimer's disease: initial report of the purification and characterization of a novel cerebrovascular amyloid protein. *Biochem. Biophys. Res. Commun* **120**, 885–890.

Gong J. S., Sawamura N., Zou K., Sakai J., Yanagisawa K. and Michikawa M. (2002) Amyloid β-protein affects cholesterol metabolism in cultured neurons: implications for pivotal role of cholesterol in the amyloid cascade. *J. Neurosci. Res.* **70**, 438–446.

Gotz J., Chen F., van Dorpe J. and Nitsch R. M. (2001) Formation of neurofibrillary tangles in P3011 tau transgenic mice induced by Aβ 42 fibrils. *Science* **293**, 1491–1495.

Hasegawa K., Yamaguchi I., Omata S., Gejyo F. and Naiki H. (1999) Interaction between Aβ (1–42) and Aβ (1–40) in Alzheimer's β-amyloid fibril formation *in vitro*. *Biochemistry* **38**, 15514–15521.

Hilbich C., Kisters-Woike B., Reed J., Masters C. L. and Beyreuther K. (1992) Substitutions of hydrophobic amino acids reduce the

amyloidogenicity of Alzheimer's disease βA4 peptides. *J. Mol. Biol.* **228**, 460–473.

Holcomb L., Gordon M. N., McGowan E. *et al.* (1998) Accelerated Alzheimer-type phenotype in transgenic mice carrying both mutant amyloid precursor protein and presenilin 1 transgenes. *Nat. Med.* **4**, 97–100.

Holtzman D. M., Bales K. R., Wu S., Bhat P., Parsadanian M., Fagan A. M., Chang L. K., Sun Y. and Paul S. M. (1999) Expression of human apolipoprotein E reduces amyloid-β deposition in a mouse model of Alzheimer's disease. *J. Clin. Invest.* **103**, R15–R21.

Hsiao K., Chapman P., Nilsen S., Eckman C., Harigaya Y., Younkin S., Yang F. and Cole G. (1996) Correlative memory deficits, Abeta elevation, and amyloid plaques in transgenic mice. *Science* **274**, 99–102.

Huang X., Atwood C. S., Moir R. D., Hartshorn M. A., Vonsattel J. P., Tanzi R. E. and Bush A. I. (1997) Zinc-induced Alzheimer's Aβ1–40 aggregation is mediated by conformational factors. *J. Biol. Chem.* **272**, 26464–26470.

Huang X., Atwood C. S., Hartshorn M. A. *et al.* (1999a) The Aβ peptide of Alzheimer's disease directly produces hydrogen peroxide through metal ion reduction. *Biochemistry* **38**, 7609–7616.

Huang X., Cuajungco M. P., Atwood C. S. *et al.* (1999b) Cu(II) potentiation of alzheimer Aβ neurotoxicity. Correlation with cell-free hydrogen peroxide production and metal reduction. *J. Biol. Chem.* **274**, 37111–37116.

Iwata N., Tsubuki S., Takaki Y., Shirotani K., Lu B., Gerard N. P., Gerard C., Hama E., Lee H. J. and Saido T. C. (2001) Metabolic regulation of brain Aβ by neprilysin. *Science* **292**, 1550–1552.

Iwatsubo T., Odaka A., Suzuki N., Mizusawa H., Nukina N. and Ihara Y. (1994) Visualization of Aβ42 (43) and Aβ40 in senile plaques with end-specific Ab monoclonals: evidence that an initially deposited species is Aβ42(43). *Neuron* **13**, 45–53.

Kontush A., Berndt C., Weber W., Akopyan V., Arlt S., Schippling S. and Beisiegel U. (2001) Amyloid-β is an antioxidant for lipoproteins in cerebrospinal fluid and plasma. *Free Radic. Biol. Med.* **30**, 119–128.

Kourie J. I. and Henry C. L. (2001) Protein aggregation and deposition: implications for ion channel formation and membrane damage. *Croat. Med. J.* **42**, 359–374.

LeVine H., 3rd. (1995) Soluble multimeric Alzheimer β(1–40) pre-amyloid complexes in dilute solution. *Neurobiol. Aging* **16**, 755–764.

LeVine H., 3rd. (1999) Quantification of β-sheet amyloid fibril structures with thioflavin T. *Meth. Enzymol.* **309**, 274–284.

Lorenzo A. and Yankner B. A. (1994) b-Amyloid neurotoxicity requires fibril formation and is inhibited by Congo red. *Proc. Natl Acad. Sci. USA* **91**, 12243–12247.

Masters C. L., Simms G., Weinman N. A., Multhaup G., McDonald B. L. and Beyreuther K. (1985a) Amyloid plaque core protein in Alzheimer disease and Down syndrome. *Proc. Natl Acad. Sci. USA* **82**, 4245–4249.

Masters C. L., Multhaup G., Simms G., Pottgiesser J., Martins R. N. and Beyreuther K. (1985b) Neuronal origin of a cerebral amyloid: neurofibrillary tangles of Alzheimer's disease contain the same protein as the amyloid of plaque cores and blood vessels. *EMBO J.* **4**, 2757–2763.

Mattson M. P., Tomaselli K. J. and Rydel R. E. (1993) Calcium-destabilizing and neurodegenerative effects of aggregated beta-amyloid peptide are attenuated by basic FGF. *Brain Res.* **621**, 35–49.

Michikawa M. and Yanagisawa K. (1998) Apolipoprotein E4 induces neuronal cell death under conditions of suppressed de novo cholesterol synthesis. *J. Neurosci. Res.* **54**, 58–67.

Michikawa M., Gong J. S., Fan Q. W., Sawamura N. and Yanagisawa K. (2001) A novel action of Alzheimer's amyloid b-protein (Aβ): oligomeric Aβ promotes lipid release. *J. Neurosci.* **21**, 7226–7235.

Mucke L., Masliah E., Yu G. Q., Mallory M., Rockenstein E. M., Tatsuno G., Hu K., Kholodenko D., Johnson-Wood K. and McConlogue L. (2000) High-level neuronal expression of Aβ1–42 in wild-type human amyloid protein precursor transgenic mice: synaptotoxicity without plaque formation. *J. Neurosci.* **20**, 4050–4058.

Naiki H., Hasegawa K., Yamaguchi I., Nakamura H., Gejyo F. and Nakakuki K. (1998) Apolipoprotein E and antioxidants have different mechanisms of inhibiting Alzheimer's β-amyloid fibril formation *in vitro*. *Biochemistry* **37**, 17882–17889.

Opazo C., Huang X., Cherny R. A. *et al.* (2002) Metalloenzyme-like activity of Alzheimer's disease b-amyloid. Cu-dependent catalytic conversion of dopanime, cholesterol, and biological reducing agents to neurotoxic H2O2. *J. Biol. Chem.* **277**, 40302–40308.

Pike C. J., Burdick D., Walencewicz A. J., Glabe C. G. and Cotman C. W. (1993) Neurodegeneration induced by β-amyloid peptides *in vitro*: the role of peptide assembly state. *J. Neurosci.* **13**, 1676–1687.

Roher A. E., Lowenson J. D., Clarke S., Woods A. S., Cotter R. J., Gowing E. and Ball M. J. (1993) β-amyloid-(1–42) is a major component of cerebrovascular amyloid deposits: implications for the pathology of Alzheimer disease. *Proc. Natl Acad. Sci. USA* **90**, 10836–10840.

Scheuner D., Eckman C., Jensen M. *et al.* (1996) Secreted amyloid β-protein similar to that in the senile plaques of Alzheimer's disease is increased *in vivo* by the presenilin 1 and 2 and APP mutations linked to familial Alzheimer's disease. *Nat. Med.* **2**, 864–870.

Simmons L. K., May P. C., Tomaselli K. J. *et al.* (1994) Secondary structure of amyloid β-peptide correlates with neurotoxic activity *in vitro*. *Mol. Pharmacol.* **45**, 373–379.

Soto C., Sigurdsson E. M., Morelli L., Kumar R. A., Castano E. M. and Frangione B. (1998) β-Sheet breaker peptides inhibit fibrillogenesis in a rat brain model of amyloidosis: implications for Alzheimer's therapy. *Nat. Med.* **4**, 822–826.

Suzuki N., Cheung T. T., Cai X. D., Odaka A., Otvos L. Jr, Eckman C., Golde T. E. and Younkin S. G. (1994) An increased percentage of long amyloid β-protein secreted by familial amyloid β-protein precursor (bAPP717) mutants. *Science* **264**, 1336–1340.

Tomita T., Maruyama K., Saido T. C. *et al.* (1997) The presenilin 2 mutation (N141I) linked to familial Alzheimer disease (Volga German families) increases the secretion of amyloid β-protein ending at the 42nd (or 43rd) residue. *Proc. Natl Acad. Sci. USA* **94**, 2025–2030.

Urbanc B., Cruz L., Le R., Sanders J., Ashe K. H., Duff K., Stanley H. E., Irizarry M. C. and Hyman B. T. (2002) Neurotoxic effects of thioflavin S-positive amyloid deposits in transgenic mice and Alzheimer's disease. *Proc. Natl Acad. Sci. USA* **99**, 13990–13995.

Vigo-Pelfrey C., Lee D., Keim P., Lieberburg I. and Schenk D. B. (1993) Characterization of β-amyloid peptide from human cerebrospinal fluid. *J. Neurochem.* **61**, 1965–1968.

Walsh D. M., Klyubin I., Fadeeva J. V., Cullen W. K., Anwyl R., Wolfe M. S., Rowan M. J. and Selkoe D. J. (2002) Naturally secreted oligomers of amyloid β-protein potently inhibit hippocampal long-term potentiation *in vivo*. *Nature* **416**, 535–539.

Yan R., Bienkowski M. J., Shuck M. E. *et al.* (1999) Membrane-anchored aspartyl protease with Alzheimer's disease β-secretase activity. *Nature* **402**, 533–537.

Yanagisawa K., Odaka A., Suzuki N. and Ihara Y. (1995) GM1 ganglioside-bound amyloid β-protein (Aβ): a possible form of pre-amyloid in Alzheimer's disease. *Nat. Med.* **1**, 1062–1066.

Yankner B. A., Duffy L. K. and Kirschner D. A. (1990) Neurotrophic and neurotoxic effects of amyloid β-protein: reversal by tachykinin neuropeptides. *Science* **250**, 279–282.

Yip C. M., Elton E. A., Darabie A. A., Morrison M. R. and McLaurin J. (2001) Cholesterol, a modulator of membrane-associated Aβ-fibrillogenesis and neurotoxicity. *J. Mol. Biol.* **311**, 723–734.

Younkin S. G. (1995) Evidence that Aβ42 is the real culprit in Alzheimer's disease. *Ann. Neurol.* **37**, 287–288.

Zou K., Gong J. S., Yanagisawa K. and Michikawa M. (2002) A novel function of monomeric amyloid β-protein serving as an antioxidant molecule against metal-induced oxidative damage. *J. Neurosci.* **22**, 4833–4841.

Journal of Neurochemistry, 2003, **84**, 1086–1096 doi:10.1046/j.1471-4159.2003.01596.x

Promotion of tau phosphorylation by MAP kinase Erk1/2 is accompanied by reduced cholesterol level in detergent-insoluble membrane fraction in Niemann–Pick C1-deficient cells

Naoya Sawamura,*,† Jian-Sheng Gong,*,‡ Ta-Yuan Chang,§ Katsuhiko Yanagisawa* and Makoto Michikawa*,¶

**Department of Dementia Research, National Institute for Longevity Sciences, Obu, Aichi, Japan*

†Japan Society for the Promotion of Science (JSPS), Tokyo, Japan

‡Organization for Pharmaceutical Safety and Research of Japan, Tokyo, Japan

§Department of Biochemistry, Dartmouth Medical School, Hanover, New Hampshire, USA

Abstract

Niemann–Pick type C (NPC) disease is a cholesterol-storage disease accompanied by neurodegeneration with the formation of neurofibrillary tangles, the major component of which is the hyperphosphorylated tau. Here, we examined the mechanism underlying hyperphosphorylation of tau using mutant Chinese hamster ovary (CHO) cell line defective in NPC1 (CT43) as a tool. Immunoblot analysis revealed that tau was hyperphosphorylated at multiple sites in CT43 cells, but not in their parental cells (25RA) or the wild-type CHO cells. In CT43 cells, mitogen-activated protein (MAP) kinase Erk1/2 was activated and the specific MAPK inhibitor, PD98059, attenuated the hyperphosphorylation of tau. The amount of protein phosphatase 2A not bound to microtubules was decreased in CT43 cells. CT43 cells but not 25RA cells were amphotericin B-resistant, indicating that cholesterol level in the plasma membrane of CT43 is decreased. In addition, the level of cholesterol in the detergent-insoluble, low-density membrane (LDM) fraction of CT43 cells was markedly reduced compared with the other two types of CHO cells. As LDM domain plays critical role in signaling pathways, these results suggest that the reduced cholesterol level in LDM domain due to the lack of NPC1 may activate MAPK, which subsequently promotes tau phosphorylation in NPC1-deficient cells.

Keywords: Alzheimer's disease, cholesterol, MAP kinase, Niemann–Pick type C, protein phosphase 2A, tau phosphorylation.

J. Neurochem. (2003) **84,** 1086–1096.

Niemann–Pick type C (NPC) disease is an autosomal recessive neurovisceral storage disorder that presently has no therapeutic cure. It is characterized by an accumulation of cholesterol and other lipids in most tissues and progressive neurodegeneration marked by premature neuronal death (Pentchev *et al.* 1995). It affects children who carry homogenous forms of the mutant *NPC1* gene (Carstea *et al.* 1997) and causes death before adulthood. The hallmark of NPC is an intracellular accumulation of free cholesterol and other lipids such as sphingolipids, which can be demonstrated as numerous polymorphous inclusions by electron microscopy, due to a defect in the sorting/trafficking of cholesterol from lysosomes and late endosomes (Pentchev *et al.* 1995; Kobayashi *et al.* 1999; Cruz *et al.* 2000). It is widely believed that the intracellular accumulation of cholesterol is mainly caused by the defective transportation of low-density

Received October 9, 2002; revised manuscript received November 12, 2002; accepted November 15, 2002.

Address correspondence and reprint requests to Makoto Michikawa, Department of Dementia Research, National Institute for Longevity Sciences, 36–3 Gengo, Morioka, Obu, Aichi 474–8522, Japan.
E-mail: michi@nils.go.jp

Abbreviations used: AD, Alzheimer's disease; CHO, Chinese hamster ovary; DMEM, Dulbecco's modified Eagle's medium; ECL, enhanced chemiluminescence; Erk, extracellular signal-regulated kinase; FBS, fetal bovine serum; GSK-3β, glycogen synthase kinase-3β; LDL, low-density lipoprotein; LDM, low-density, detergent-insoluble membrane; LPDS, lipoprotein-deficient fetal calf serum; MAPK, mitogen-activated protein kinase; NFT, neurofibrillary tangle; PHF, paired helical filaments; NPC, Niemann–Pick type C; PBS, phosphate-buffered saline; PP2A, protein phosphatase 2A; SCAP, SREBP cleavage-activating protein; SDS–PAGE, sodium dodecyl sulfate–polyacrylamide gel electrophoresis; SREBP, sterol regulatory element binding protein; TS, Tris-saline.

lipoprotein (LDL)-derived cholesterol from the hydrolytic organelle in NPC cells (Blanchette-Mackie *et al.* 1988; Liscum *et al.* 1989; Xie *et al.* 1999a). Recent studies, however, have shown that endogenously synthesized cholesterol can also contribute to cholesterol accumulation as a result of the circulation of cholesterol between the plasma membrane and endosomal/lysosomal compartments (Cruz and Chang 2000; Lange *et al.* 2000).

Mutations in *NPC1* are known to cause neurological disorders including ataxia, dystonia, and dementia. In addition to neuronal storage and neurodegeneration, the formation of neurofibrillary tangles (NFTs) without amyloid deposits has been noted in NPC brains (Auer *et al.* 1995; Love *et al.* 1995; Suzuki *et al.* 1995). The presence of NFTs, which are composed of paired helical filaments (PHF), is also known as one of the diagnostic hallmarks of Alzheimer's disease (AD; Goedert *et al.* 1996). The major component of PHF is hyperphosphorylated tau, which is a microtubule-associated protein (Grundke-Iqbal *et al.* 1986b; Nukina and Ihara 1986). It has previously been shown that the phosphorylation of tau prevents it from binding to microtubules (Grundke-Iqbal *et al.* 1986b; Wood *et al.* 1986; Kosik *et al.* 1988; Lee *et al.* 1991; Goedert *et al.* 1992b). Although the phosphorylation of tau in AD is the subject of intense investigation, the molecular mechanism responsible for this altered regulation remains to be determined. Since the involvement of cholesterol in the pathogenesis of AD has been highlighted (Hartmann 2001; Simons *et al.* 2001), it is noteworthy that a perturbation in cholesterol metabolism and NFT formation without amyloid deposits coexist in the brains of NPC patients. This may indicate that a disturbance in cholesterol metabolism is responsible for tauopathy not only in NPC but also in AD. In support of this assumption, recent studies have demonstrated that amyloid β-protein affects cholesterol metabolism (Liu *et al.* 1998; Michikawa *et al.* 2001) and disrupts its homeostasis in neurons (Gong *et al.* 2002), and that altered cholesterol metabolism induces tau phosphorylation in cultured neurons with axonal degeneration associated with microtubule depolymerization (Fan *et al.* 2001) and in mouse brains (Koudinov and Koudinova 2001). These findings suggest a pivotal role of cholesterol in a mechanism that promotes tau phosphorylation. We have recently reported that hyperphosphorylated tau and enhanced mitogen-activated protein kinase (MAPK) activity are found in brains of NPC mice (Sawamura *et al.* 2001); however, the direct cause and result relationship between enhanced MAPK activity and tau phosphorylation in NPC1 mice remains unclear, and the mechanisms promoting MAPK activity and tau phosphorylation in NPC1-deficient neurons and in neurons whose cholesterol metabolism is disrupted remains to be elucidated. These lines of evidence naturally lead us to a question as to which factor, cholesterol accumulation, cholesterol shortage due to lack of its trafficking, or other mechanism related to NPC1 deficiency is critical for promotion of MAPK activity and subsequent induction of tau phosphorylation.

Previous studies have demonstrated a crucial role of NPC1 in cholesterol metabolism using a mutant Chinese hamster ovary (CHO) cell line, CT43, that is deficient in NPC1 due to premature termination of its translation (Liscum and Klansek 1998; Neufeld *et al.* 1999; Cruz and Chang 2000; Cruz *et al.* 2000; Millard *et al.* 2000). The use of the cell models for NPC such as CT43 could provide important insights into not only the role of NPC1 in cholesterol metabolism, but also that of NPC1 and/or cholesterol in the expression of various phenotypes observed in NPC including tau phosphorylation. Therefore, to fully understand the molecular mechanisms underlying tau phosphorylation associated with the genetic mutation in *NPC1*, we have established human tau stable transformant cell lines from NPC1-deficient CT43 cell line and their parental cell line 25RA (Chang and Limanek 1980; Hua *et al.* 1996). In this study, we characterized the distribution of cholesterol in LDM fraction in NPC1-deficient cells and investigated the involvement of tau-directed kinase, MAPK, and protein phosphatase 2A (PP2A) in the promotion of tau phosphorylation in these cells. We found that the distribution of cholesterol in LDM fraction is markedly reduced, and that tau is hyperphosphorylated at multiple sites in NPC1-deficient cells, which is induced by highly activated MAPK and an increased amount of an inactive form of PP2A.

Experimental procedures

Materials

Amphotericin B, mevalonic acid, mevastatin (compactin), and 3-(4,5-dimethylthiazal-2-yl)-2,5-diphenyltetrazolium bromide (MTT) were purchased from Sigma (St Louis, MO, USA). MAP kinase inhibitor, PD98059, was purchased from Promega (Madison, WI, USA). The monoclonal antibody Tau-1 was obtained from Chemicon International (Temecula, CA, USA). The monoclonal antibodies, PHF-1 and CP13, were kindly provided by Dr P. Davies (Albert Einstein College of Medicine). The monoclonal antibodies AT-100 and AT-180, were purchased from Innogenetics (Ghent, Belgium). The monoclonal antibody T46 was obtained from Zymed Laboratories (San Francisco, CA, USA). Rabbit polyclonal anti-phospho-MAPK (specific for Thr-202/Tyr-204 phosphorylation) and antiphospho-independent-MAPK antibodies, which recognize anti-phospho-extracellular signal-regulated kinase 1/2 (Erk1/2) and antiphospho-independent Erk1/2, respectively, and mouse monoclonal antibody against phospho-GSK-3β (specific for serine-9 phosphorylation) were purchased from Cell Signaling Technology (Beverly, MA, USA). The monoclonal antibody against pan-GSK-3β was obtained from Transduction Laboratories (Lexington, KY, USA). The monoclonal antibody against β-tubulin, DM1A, was obtained from Sigma. The monoclonal antibodies against phospho-GSK3β (specific for tyrosine-216 phosphorylation) and protein phosphatase 2A (PP2A) were purchased from Upstate Biotechnology (Lake Placid, NY, USA).

Construction of expression plasmids for transfection

Four-repeat (4R)-tau cDNAs were amplified from human adult cDNA libraries, and ligated with pCR 2.1 using the Original TA Cloning kit (Invitrogen Corp., Carlsbad, CA, USA). The *Eco*RI fragment containing 4R-tau was isolated and ligated with pcDNA3 digested with the same endonuclease. The resultant recombinant plasmid, pcDNA3–4R-tau, was used for further studies. The entire nucleotide sequence was determined by the dideoxynucleotide termination method using a DNA sequencer. Vectors containing 4R-tau cDNA were transfected into each CHO cell line (wild-type, 25RA, or CT43) using a Polyfect Transfection reagent (Qiagen, Hilden, Germany) according to the manufacturer's instructions. Clones that survived in Geneticin (Life Technologies, Rockville, MD, USA; 0.6 mg/mL) were isolated and maintained in Ham's F12 medium (Life Technologies) supplemented with 10% fetal bovine serum (FBS) containing 0.6 mg/mL Geneticin at 37°C in 5% CO_2.

Protein preparation

Cultured cells grown in 10-cm dishes were scraped off and suspended in ice-cold Tris–saline [TS; 50 mM Tris–HCl (pH 7.4), 150 mM NaCl], containing protease inhibitors (Complete™), followed by homogenization using a motor-driven Teflon homogenizer. The homogenates were centrifuged at 3000 *g* for 10 min at 4°C and supernatants were collected for biochemical analyses. Protein concentrations were determined using the bicinchoninic acid protein assay kit (Pierce, Rockford, IL, USA). Aliquots of the supernatant samples containing equal amounts of protein were subjected to sodium dodecylsulfate–polyacrylamide gel electrophoresis (SDS–PAGE) for immunoblot analysis as described previously (Sawamura *et al.* 2001).

Lipid analysis

Cells of each cell line were seeded in 6-well culture dishes in medium A (Ham's F-12 containing 10% FBS). Twenty-four hours after plating, the cells were washed twice with phosphate-buffered saline (PBS) and refed with medium A or B [Ham's F-12 containing 5% (v/v) lipoprotein-deficient fetal calf serum (LPDS; Sigma)] and maintained for another 2 days, followed by washing with PBS three times and drying at room temperature. Extraction of lipids and subsequent determination of the amount of cholesterol and phospholipids in each sample were carried out according to previously described methods (Michikawa *et al.* 2000). In brief, lipids in the samples were extracted by hexane/isopropyl alcohol (3 : 2, v/v), and evaporated under N_2 gas. The amount of total cholesterol was determined using a cholesterol determination kit, LTCII (Kyowa Medex, Tokyo, Japan), and that of free cholesterol was determined using LFC (Kyowa Medex). The amount of phospholipids was determined using a phospholipid determination kit, PLB (Wako, Osaka, Japan). The amount of cholesteryl esters was determined by subtracting free cholesterol from total cholesterol. After extraction of lipids, proteins in the samples were isolated using 0.1 N NaOH solution and the cellular protein concentrations were determined using the bicinchoninic acid protein assay kit (Pierce) using bovine serum albumin as the standard. The amounts of cholesterol and phospholipids/mg protein in each sample were then calculated.

Quantification of intracellular lipids by [^{14}C]acetate labeling

On day 0, cells of each cell line were seeded in medium A in 6-well culture dishes. On day 1, the cells were washed twice with PBS and re-fed with medium A or B. On day 3, the cells were pulsed with 37 kBq/mL [^{14}C]acetate (DuPont NEN) for 2 h. Lipids were extracted and separated by TLC, and the amounts of [^{14}C]acetate incorporated into cholesterol, phosphatidylcholine, and cholesteryl esters were quantified using Bio-Imaging-Analyzer System-2500 (Fuji Photo Film Co., Ltd, Tokyo, Japan) as previously described (Michikawa and Yanagisawa 1998, 1999).

Immunoblot analysis

Proteins separated using SDS–PAGE were electrophoretically transferred onto a polyvinylidene difluoride (PVDF) membrane (Millipore, Bedford, MA, USA). Non-specific binding was blocked with 5% fat-free milk in PBS containing 0.1% Tween-20. The blots were then incubated with primary antibodies overnight at 4°C. For the detection of both monoclonal and polyclonal antibodies, appropriate peroxidase-conjugated secondary antibodies were used in conjunction with SuperSignal Chemiluminesence (Pierce) to obtain images saved on film. The primary antibodies used were as follows: Tau-1, diluted 1 : 1000; PHF-1, diluted 1 : 20; CP13, diluted 1 : 20; AT-100, diluted 1 : 500; AT-180, diluted 1 : 500; T46, diluted 1 : 2500; antiphospho-Erk1/2 antibody, diluted 1 : 1000; antiphospho-independent Erk1/2 antibody, diluted 1 : 1000; antiphospho-GSK-3β antibody (specific for serine-9 phosphorylation), diluted 1 : 1000; antiphospho-GSK-3β antibody (specific for tyrosine-216 phosphorylation), diluted 1 : 500; antipan-GSK3β antibody, diluted 1 : 2500; antiβ-tubulin antibody, diluted 1 : 500 and antiprotein phosphatase 2A (PP2A) antibody, diluted 1 : 1000.

Immunoblot detection of protein associated with microtubule polymers and soluble tubulin

Soluble tubulin and insoluble microtubule polymers were obtained by scraping of cells of each cell line from 10-cm dish and suspended in 250 μL of microtubule-stabilizing buffer, i.e. PME buffer containing 2 mM GTP, 0.1% Triton X-100, 2 mM dithiothreitol, and a mixture of protease inhibitors, Complete™. The scraped off material in PME buffer was homogenized using a motor-driven Teflon homogenizer. The homogenate was centrifuged at 1000 *g* for 10 min at 30°C and the supernatant was obtained for further analyses. Protein concentrations were determined using the bicinchoninic acid protein assay kit (Pierce). Aliquots of the supernatant containing equal amounts of protein were subjected to centrifugation at 204 000 *g* for 60 min at 30°C, resulting in the generation of a supernatant fraction containing soluble tubulin and a pellet fraction containing microtubule polymers. The pellet fractions were solubilized in SDS buffer [63.5 mM Tris–HCl buffer (pH 6.8), containing 2% SDS] at 4°C, followed by sonication to release proteins bound to microtubules, and then heated at 90°C for 10 min under reductive conditions. The samples were then centrifuged at 20 630 *g* for 5 min and the clear supernatant was subjected to SDS–PAGE for immunoblot analysis as described previously (Sawamura *et al.* 2001).

Amphotericin B killing

The effect of amphotericin B on cell killing of CHO cells (wild-type, 25RA, or CT43) was performed according the method described

previously (Underwood *et al.* 1998). On day 0, each CHO cell line was seeded in 96-well plates in Ham's F12 medium containing 10% FBS (medium A). On the next day, the culture medium was changed to Ham's F12 medium containing 5% LPDS (medium B). On day 2, each cell line cells were re-fed medium B plus 20 μM compactin, an HMG-CoA reductase inhibitor, and 0.1 mM mevalonate. On day 3, cells were incubated with Ham's F12 medium containing 1% LPDS with or without 100 μg/mL amphotericin B. After 5 h, cells were washed with Hank's balanced salt solution (Life Technologies) three times. Cell viability was determined using a colorimetric MTT assay as previously reported (Isobe *et al.* 1999).

Purification of detergent-insoluble, low-density membrane fraction

LDM fraction was obtained from CHO cells according to an established method previously reported (Lisanti *et al.* 1994; Sawamura *et al.* 2000). One milliliter of each fraction was sequentially collected from the top of the gradient. Extraction of lipids and subsequent determination of the amount of cholesterol and phospholipid in each sample were carried out according to previously described methods (Michikawa *et al.* 2000).

Detection of GM1 ganglioside

For detection of GM1 ganglioside, samples of each fraction were dissolved in equal volume of Laemmli buffer. They were then subjected to 4–20% gradient Tris–tricine SDS–PAGE (Dai-ichi Pure Chemical Co., Ltd, Tokyo, Japan). The separated GM1 ganglioside was transferred onto an immobilon or polyvinylidene difluoride membrane (Millipore) with a semidry electrophoretic transfer apparatus (Nihon Eido, Tokyo, Japan) using a transfer buffer (0.1 M Tris, 0.192 M glycine, and 20% methanol). The membranes were blocked with 5% fat-free milk in PBS containing 0.1% Tween-20 for 1 h, and probed with horseradish peroxidase-conjugated cholera toxin B (Sigma; final concentration at 42 ng/mL) overnight at 4°C. In between steps, the membranes were washed four times with PBS-T for 15 min. Bound cholera toxin was detected using Super Signal Chemiluminescence (Pierce).

Statistical analysis

Statistical analysis was carried out using StatView computer software (Macintosh version 5.0, Abacus Concepts Inc., Berkeley, CA, USA). P-value < 0.05 were considered to be significant.

Results

We analyzed the role of intracellular cholesterol in tau phosphorylation by mainly using two CHO cell lines (25RA, CT43; Cruz and Chang 2000; Cruz *et al.* 2000). To study the phosphorylation of tau in these CHO cell lines, 4R tau was stably transfected, because CHO cells do not normally express tau. After transfection, several clones were screened for tau expression by western blotting of the post-nuclear fraction with a T46 antibody, which recognizes phospho-independent tau. Among the cell lines obtained, clone 7 in tau-transfected 25RA cells and clone 25 in tau-transfected CT43 cells have similar expression levels of tau (data not shown). Thus, we used these two lines for further studies.

We examined the features of cholesterol metabolism in 25RA and CT43 cells remain unchanged after transfection with human tau. The ratio of free cholesterol to total cholesterol significantly increased in CT43 cells compared to 25RA cells (Fig. 1a). In contrast, the concentrations of cholesteryl esters in CT43 cells markedly decreased compared to those in 25RA cells (Fig. 1b). The concentrations of cholesteryl esters in CT43 cells remained at very low levels even when the cells were cultured in 10% FBS (27.8 μg/mL cholesterol) (Fig. 1b). The rate of *de novo* cholesterol

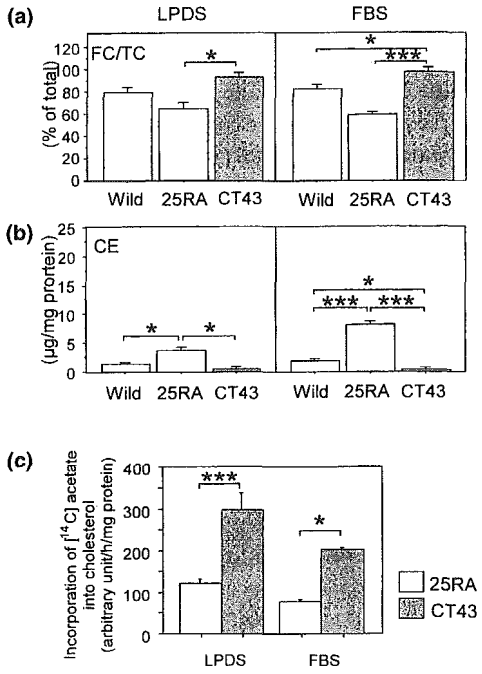

Fig. 1 Determination of concentrations of cholesterol and cholesteryl ester, and synthesis of cholesterol in wild-type CHO, 25RA, and CT43 cells expressing human tau. (a and b) Cells of each cell line were seeded in medium A in 6-well culture dishes. Twenty-four hours after plating, the cells were washed twice with PBS and re-fed with medium A or B and maintained for another 2 days, followed by washing with PBS three times and drying at room temperature. Lipids were extracted from each cell line and the concentrations of total and free cholesterol in each sample were determined according to the procedures described in Experimental procedures. The protein concentrations in each sample were determined and the concentrations of each lipid in the samples were calculated. The ratio of free cholesterol to total cholesterol was calculated (a) and the amounts of cholesteryl esters were determined by subtracting free cholesterol from total cholesterol (b). (c) Cells were plated in medium A in 6-well plates. On day 1, the media were replaced with medium A or medium B. On day 3, the cells were pulsed with [^{14}C]acetate for 2 h. Lipids were extracted and analyzed by TLC, and amounts of [^{14}C]acetate incorporated into cholesterol were quantified. Values are means ± SE, $n = 6$ for each culture. Three independent experiments showed similar results. $^{*}p < 0.05$ and $^{***}p < 0.0001$.

synthesis in CT43 cells was 2.5- and 3.0-fold higher than that in 25RA cells in 10% FBS-containing media or 5% LPDS-containing media, respectively (Fig. 1c). Cholesterol accumulation as demonstrated by filipin staining and electric microscopy was observed only in CT43 expressing tau (data not shown). These results are similar to those reported in CT43 cells not transfected with tau (Cruz and Chang 2000; Cruz *et al.* 2000) and in tissues of NPC mice (Xie *et al.* 1999a,b), indicating that the overexpression of tau in CT43 cells also has similar features of cholesterol metabolism to those of NPC1-deficient cells and tissues, which defects sorting and trafficking of cholesterol from lysosomes and late endosomes (Pentchev *et al.* 1995; Kobayashi *et al.* 1999; Cruz *et al.* 2000).

We next examined the phosphorylation state of tau in wild-type CHO, 25RA, and CT43 cells using several well-characterized antibodies, which recognize site-specific phosphorylation of tau. Results of the immunoblot analysis of tau using the Tau-1 antibody show that tau in the three cell lines were found to have apparent molecular masses between 49 and 61 kDa (Fig. 2). For samples derived from CT43 cells, the main bands immunoreactive to Tau-1, which recognizes tau non-phosphorylated at four nearby serine residues at 195, 198, 199, and 202, appear to exhibit slower electrophoretic mobility (Fig. 2, upper arrow) than the bands for samples derived from wild-type and 25RA cells (Fig. 2, signals between the two arrows). These bands of tau exhibiting slower mobility are known to be characteristic of phosphorylated tau. Next, we used the site-specific phosphorylation-dependent antibodies PHF1, AT-180, AT-100, and CP13 that recognize the phosphorylated tau epitopes, Ser396/Ser404, Thr231, Ser214/Thr217, and Ser202, respectively. The upper migrating band representing tau was strongly reactive to antibodies, PHF-1, AT180, AT-100, and CP13, when samples from CT43 cells were analyzed. This was not observed when samples from the wild-type CHO and 25RA cells were analyzed (Fig. 2). In contrast, the expression level of tau detected by a phosphorylation-independent antibody, T46, was not significantly altered among these three cell lines (Fig. 2). The main bands immunoreactive to T46 for samples derived from CT43 cells exhibit slower mobility than the bands for samples derived from wild-type and 25RA cells (Fig. 2). These results indicate that tau is hyperphosphorylated at sites Ser396/Ser404, Thr231, Ser214/Thr217, and Ser202 in CT43 cells, but not in wild-type CHO and 25RA cells.

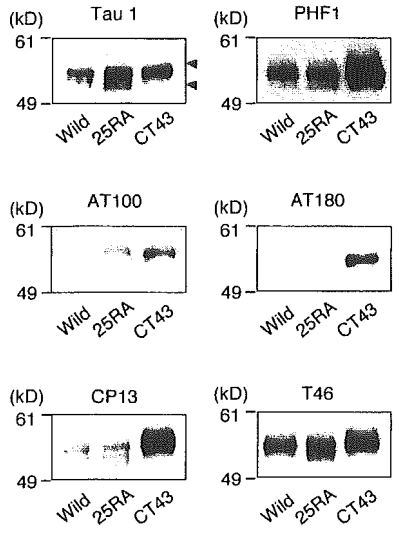

Fig. 2 Immunoblot analysis of tau in wild-type, 25RA, and CT43 CHO cells. Cells of each cell line were seeded in medium A in 10-cm culture dishes. Twenty-four hours after plating, the cells were re-fed with medium A and maintained for another 24 h, followed by washing with PBS three times and the cultured cells were harvested as described in Experimental procedures. Equivalent amounts of post-nuclear supernatant protein from wild-type, 25RA, and CT43 CHO cells were separated using 10% SDS–PAGE. The separated proteins were immunoblotted with the Tau-1 antibody and the site-specific phospho-tau antibodies, PHF-1, AT-100, and AT-180, in addition to T46, which is a phosphorylation-independent antibody. Three independent experiments showed similar results.

To determine the molecular basis for the enhanced tau phosphorylation in CT43 cells, the expression and phosphorylation state of well-known tau-directed protein kinases, including MAPK and GSK3β, were determined. Immunoblot analysis using the antiphospho-MAPK antibody, which recognizes only the activated form of Erk1 and Erk2, revealed increased amounts of the active form of MAPK (Erk1/2) in the samples from CT43 cells compared to those in the samples from wild-type and 25RA cells (Fig. 3a). The overall expression levels of MAPK were determined to be similar among the three cell lines using antiphospho-independent MAPK antibody (Fig. 3a). Immunoblot analysis using the antiphospho-GSK3β antibody (Ser9), which specifically recongnizes serine-9 phosphorylation of GSK3β, showed no alteration in the amount of inactive form of GSK3β among the three cell lines (Fig. 3a). Immunoblot analysis using the antiphospho-GSK3β antibody (Tyr216), which specifically recongnizes tyrosine-216 phosphorylation of GSK3β, showed no alteration in the amount of active form of GSK3β among the three cell lines (Fig. 3a). In addition, immunoblot analysis using antipan-GSK3β antibody (pan-GSK3β) showed no alteration in the amount of total GSK3β protein among the three cell lines (Fig. 3a). These results indicate that GSK3β is not involved in NPC1-induced tau phosphorylation. To determine whether phosphorylation of tau occurs downstream of the site of MAPK activation, we studied the effect of a highly selective inhibitor of MAPK kinase activation, PD98059 (Alessi *et al.* 1995; Dudley *et al.* 1995) on tau phosphorylation. As shown in Figs 3(b and c), PD98059 significantly inactivated MAPK and attenuated signals of

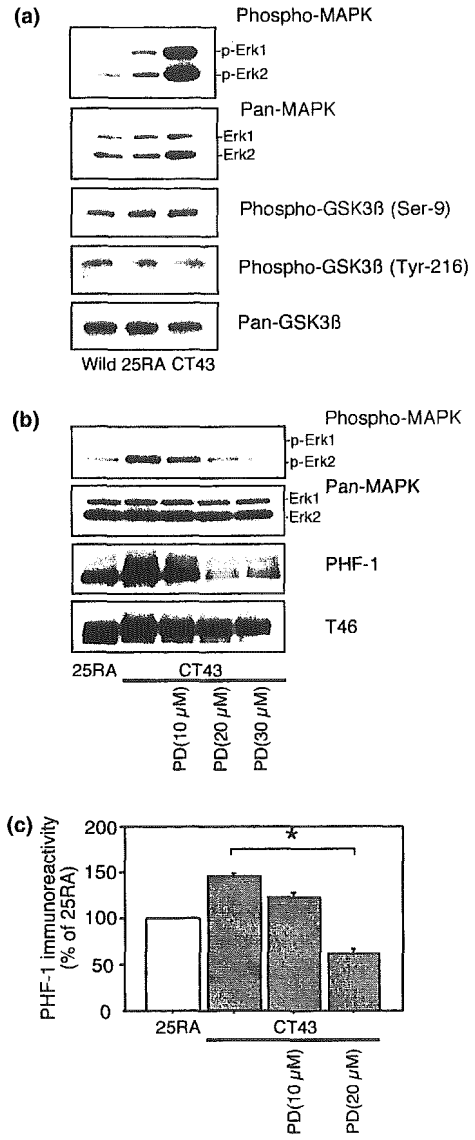

Fig. 3 Determination of phosphorylation state of MAPK and its effect on tau phosphorylation in wild-type, 25RA, and CT43 CHO cells. Cells of each cell line were seeded in medium A in 10-cm culture dishes. Twenty-four hours after plating, the cells were re-fed with medium A and maintained for another 24 h, followed by washing with PBS three times and the cultured cells were harvested as described in Experimental procedures. (a) The post-nuclear fractions of wild-type, 25RA, and CT43 CHO cells were analyzed for the activation of MAPK and phosphorylation of GSK3β. MAPK activation was determined by immunoblot analysis of post-nuclear supernatants using the anti-phospho-MAPK antibody that primarily recognizes activated Erk1/2. The total MAPK was similarly determined using the antiphosphorylation-independent Erk1/2 antibody. The level of activation of GSK-3β was determined using the antiphospho-GSK-3β antibody specific for Ser9 phosphorylation and the one specific for Tyr216 phosphorylation. The total amount of GSK3β was determined using the antiphospho-independent GSK3β antibody. (b) CT43 cells were incubated for 48 h with or without PD98059 (PD), and then the post-nuclear fractions were analyzed to determine phosphorylation states of Erk1/2 and tau using antiphospho-Erk1/2 and PHF-1 antibodies, respectively, as described in Experimental procedures. The total amount of Erk1/2 and tau in the post-nuclear fractions were determined using the antiphosphorylation-independent Erk1/2 and T46 antibodies, respectively. Four independent experiments showed similar results. (c) CT43 cells were incubated for 48 h with or without PD, and then the post-nuclear fractions were analyzed to determine phosphorylation states of tau using PHF-1 antibody. The immunoreactivity of each sample to PHF-1 antibody was quantified using a Macintosh computer with software (NIH Image) for densitometric analysis. The data are means ± SE for triplicates. $^*p < 0.01$.

the PHF-1-immunoreactive band in a dose-dependent manner in CT43 cells. These results indicate that the MAPK pathway, but not the GSK3β pathway, is responsible for the hyperphosphorylation of tau in NPC-deficient cells.

Because phosphorylation of tau has been reported to affect its ability to bind to microtubules, biochemical and morphological examinations were performed to confirm whether microtubule stability was affected by hyperphosphorylated tau in CT43 cells. Total, monomeric and polymerized forms of tubulin were extracted from three CHO cell lines and detected by immunoblot analysis. Western blot analysis using the antiβ-tubulin antibody showed that the levels of monomeric and polymeric tubulin were not altered among the three cell lines (Fig. 4a).

The phosphorylation state of tau is known to be modulated not only by kinases but also by phosphatases. Among those candidate enzymes, PP2A is one of the pivotal phosphatases regulating the phosphorylation state of tau in mouse brains (Gong *et al.* 2000; Kins *et al.* 2001) and AD brains (Vogelsberg-Ragaglia *et al.* 2001). We therefore determined the amount of PP2A bound to microtubules and that not bound to microtubules in these three cell lines, because its activity to dephosphorylate tau is ensured when PP2A is not bound to microtubules (Sontag *et al.* 1999). As shown in Fig. 4(a, pellet fraction), PP2A with an increased level was detected to be bound to microtubules in CT43 compared to 25RA. The amount of PP2A not bound to microtubules significantly decreased and that bound to microtubules significantly increased in CT43 cells (Fig. 4b, supernatant).

The results shown in Fig. 1, suggest the shortage of available cholesterol in CT43 cells, giving rise to a question of whether cholesterol deficiency in a specific compartment is responsible for the activation of MAPK leading to tau phosphorylation. To address this question, we have performed an amphotericin B test to compare the cholesterol levels in the plasma membrane among these three cell lines. Amphotericin B is a polyene antibiotic that forms pores in cholesterol-rich membranes (Norman *et al.* 1972) and its

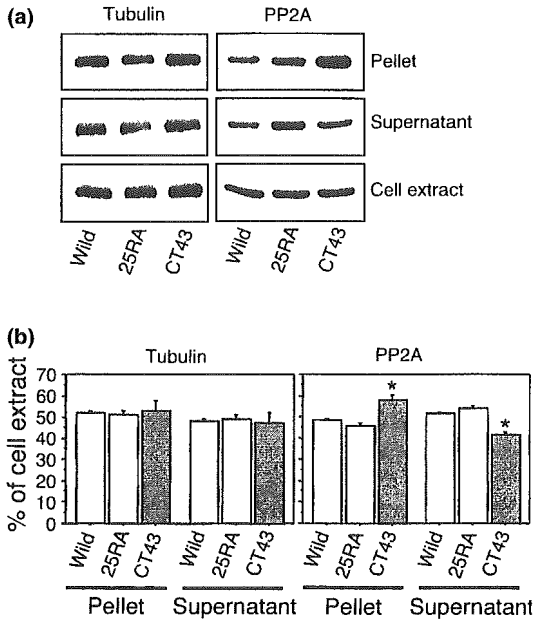

Fig. 4 Determination of the amount of PP2A bound and not bound to microtubules in wild-type, 25RA, and CT43 CHO cells. Cells of each cell line were seeded in medium A in 10-cm culture dishes. Seventy-two hours after plating, the cultured cells were harvested as described in Experimental procedures. (a) The total (cell extract), polymeric (pellet), and monomeric (supernatant) forms of tubulin were extracted from wild-type, 25RA, and CT43 CHO cells as described in Experimental procedures. Western blot analysis was carried out using antiβ-tubulin and anti-PP2A antibodies. (b) The intensity of each band was quantified using a Macintosh computer with software (NIH Image) for densitometric analysis. The data represent means ± SE, $n = 4$ for each culture. $^*p < 0.001$ versus wild-type CHO cells.

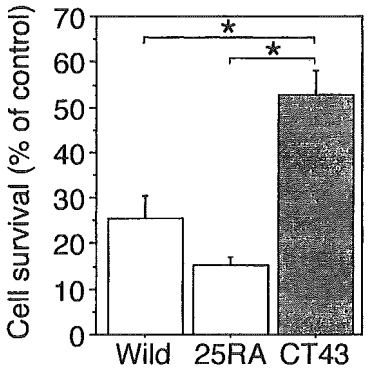

Fig. 5 Cell killing activity of amphotericin B on wild-type, 25RA, and CT43 cells. Wild-type, 25RA, and CT43 cells were grown as described in Experimental procedures. The cells were incubated in Ham's F12 medium containing 5% FBS, 20 μM compactin, and 0.1 mM mevalonate. After 16 h, the cells were treated with 100 μg/mL amphotericin B, and cell viability was determined using a colorimetric MTT assay as described in Experimental procedures. Data are expressed as cell viability ratio of sample culture to that of each control culture. The data represent means ± SE, $n = 6$ for each culture. $^*p < 0.01$.

killing action depends on the cholesterol concentration in the plasma membrane (Underwood *et al.* 1998). The ratio of CT43 cells that survived following amphotericin B treatment was significantly higher than that of 25RA cells (Fig. 5), indicating that 25RA cells are more sensitive to amphotericin B than CT43 cells. These results suggest that the cholesterol concentration in the plasma membrane of CT43 cells is lower than that of the other two types of cells.

Based on these results, we carried out experiments to determine whether NPC1 deficiency affects cholesterol distribution at specific cellular compartments such as LDM domain or detergent-insoluble, glycolipid-enriched membrane domain (DIG) due to a defect in cholesterol trafficking. DIGs are rich in sphingolipids and cholesterol and serve as membranous rafts for recruiting proteins and lipids that collaborate in signaling (Brown and London 1997; Simons and Ikonen 1997). DIGs were reported to be fractionated in a Triton X-100-insoluble, low-density fraction by sucrose density gradient ultracentrifugation (Fielding and Fielding 1995). Thus, we treated cells with Triton X-100, separated them in a sucrose density gradient, and determined the levels of cholesterol, phospholipids, and GM1, a marker for DIGs, in each fraction. As shown in Fig. 6, the low-density floating fraction (fraction 4) enriched in GM1 contained 16% and 11% of total cholesterol in wild-type CHO and 25RA cells, respectively, while only 3.8% of total cholesterol was recovered in fraction 4 of CT43 cells. In addition, in contrast to the wild-type CHO and 25RA cells, the distribution peak of cholesterol in LDM fraction was not observed in CT43 cells, while that of phospholipids and GM1 remained (Fig. 6a–c). These results suggest that the structure of LDM domain may have been altered and their function deteriorated. In support of this notion, similar results were obtained in primarily cultured neurons whose cholesterol level decreased following treatment with compactin, a 3-hydroxy-3-methyglutaryl co-enzyme A (HMG-CoA) reductase inhibitor. Cultured neurons maintained in a serum-free medium in the presence or absence of compactin were collected, treated with Triton X-100, separated in a sucrose density gradient ultracentrifugation, and then the levels of cholesterol, phospholipids, and GM1 ganglioside, a marker for DIG, in each fraction were determined. As shown in Fig. 7(a), the low-density floating fraction (fraction 5) enriched in GM1 contained 22% of total cholesterol in non-treated neurons, while only 9.6% of total cholesterol was recovered in fraction 5 of compactin-treated neurons. Moreover, the distribution peak of cholesterol in LDM fraction was not observed in cholesterol-deficient neurons, while that of GM1 remained (Fig. 7c). Consistent with the observation in CT43 cells, activation of MAP kinase was induced in cholesterol-deficient neurons (Fig. 7d) that have lost the distribution peak of cholesterol in LDM fraction. The enhancement in MAPK activity in

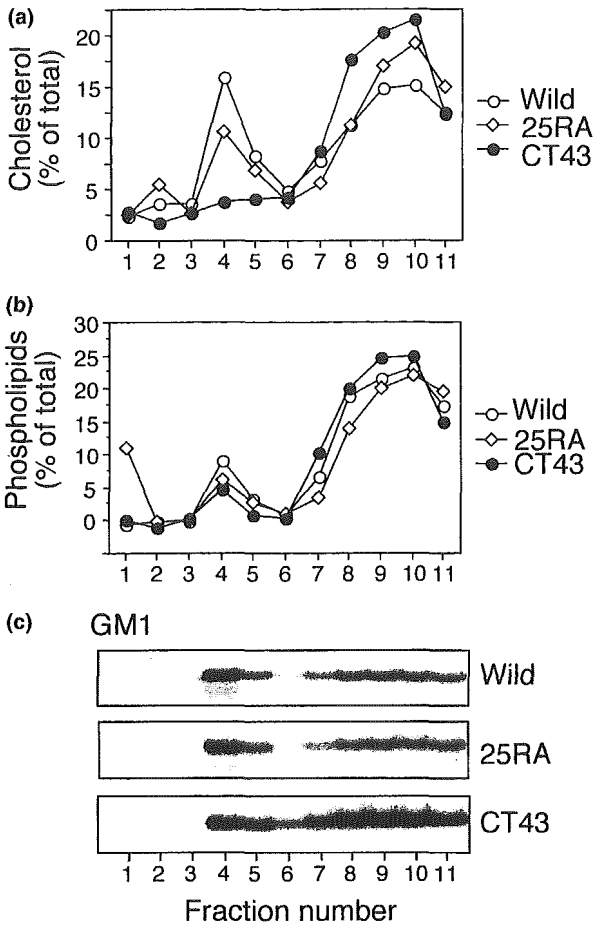

Fig. 6 Characterization of LDM fraction of wild-type CHO, 25RA, and CT43 cells. Wild-type CHO, 25RA, and CT43 cells were homogenized in the presence of 1% Triton X-100 and fractionated by sucrose density gradient centrifugation as described previously (Lisanti *et al.* 1994). Fractions were collected from the top and 11 fractions were obtained. The levels of cholesterol (a) and phospholipids (b) in each fraction were determined as described in Experimental procedures. The distribution of GM1 (c), a marker for DIG, across the fractions was determined as described in Experimental procedures. Two independent experiments showed similar results. ○, Wild-type; ◇, 25RA; ●, CT43.

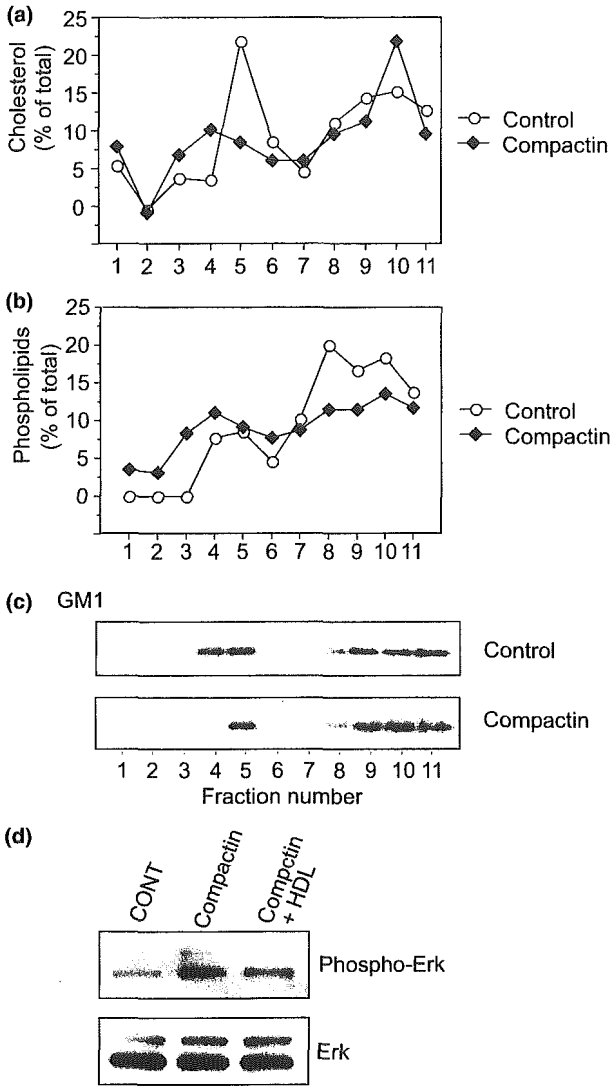

Fig. 7 Characterization of LDM fraction of cultured neurons in the presence or absence of an HMG-CoA reductase inhibitor. Neuron-rich cultures were prepared from cerebral cortices as previously described (Michikawa *et al.* 2001). The neurons were plated onto poly D-lysine-coated 6-well plates at a cell density of $2 \times 10^5/cm^2$, and maintained in a serum-free medium consisting of Dulbecco's modified Eagle's medium nutrient mixture (DMEM/F12; 50% : 50%) and N_2 supplements. Six hours after plating, some cultures were treated with 300 nM compactin. The cultures were maintained for 3 days and then harvested. The cells were then homogenized in the presence of 1% Triton X-100 and fractionated by sucrose density gradient centrifugation as described previously (Lisanti *et al.* 1994). Fractions were collected from the top and 11 fractions were obtained. The levels of cholesterol (a) and phospholipids (b) in each fraction were determined as described in Experimental procedures. The distribution of GM1 (c), a marker for DIG, across the fractions was determined as described in Experimental procedures. MAPK activation was determined by immunoblot analysis of the postnulear supernatants using antiphospho-MAPK antibody that recognizes activated Erk1/2 (d). The cells treated with compactin plus HDL were also analyzed. Two independent experiments showed similar results. ○, Control; ◆, compactin.

cholesterol-deficient neurons was prevented by the concurrent treatment with HDL (Fig. 7d).

Discussion

The experiments described here were designed to test the assumption established from previous *in vivo* experiments that altered cholesterol metabolism due to the genetic mutation in *NPC1* is responsible for the activation of the MAPK-signalling pathway, which leads to hyperphosphorylation of tau, NFT formation, and neurodegeneration in NPC (Sawamura *et al.* 2001). In this study, we elucidated the mechanism, by which alterations in cholesterol metabolism

at a specific cellular compartment due to the lack of NPC1 induce MAPK activation and subsequent tau phosphorylation. We observed the following: (i) tau is hyperphosphorylated at multiple sites, (ii) MAPK is highly activated, and (iii) the MAPK inhibitor attenuates the phosphorylation of tau in NPC1-deficient CHO cells; additionally, we found that (iv) the cholesterol level in the plasma membrane decreased and (v) the cholesterol level in LDM fraction also decreased in CT43 cells. These findings suggest that in NPC1-deficient cells, the decreased level of cholesterol in the plasma membrane with a failure in maintenance of the structure and function of LDM domain, called lipid raft or DIG, may result in the alteration in these domain-related signals including MAPK activity, leading to enhanced phosphorylation of tau.

We show that tau is hyperphosphorylated at sites, Ser202, Ser214, Thr217, Thr231, Ser396, and Ser404 in NPC1-deficient CT43 cells, which is assumed to most probably result from an imbalance of tau kinase and phosphatase activities in the cells. Among them, we have focused on MAPK and PP2A, because we have found that the activities of MAPK (Sawamura *et al.* 2001) and PP2A (our unpublished data) are altered in the brains of NPC (–/–) mice, in which tau is hyperphosphorylated. In accordance with the *in vivo* findings, tau and MAPK were highly phosphorylated in CT43 cells. The direct evidence that enhanced phosphorylation of tau in CT43 cells is attenuated by a MAPKK inhibitor, PD98059, indicates that activated MAPK is responsible for promoting tau phosphorylation. Additionally, we show that the amount of PP2A not bound to microtubules is decreased in CT43 cells compared to that of 25RA cells. The catalytic subunit of PP2A is inhibited by its binding to microtubules, which could be a competitive inhibitor of PP2A in binding to the same region on tau (Sontag *et al.* 1999), suggesting that PP2A can efficiently dephosphorylate tau only when neither protein is bound to microtubules. Thus, it is possible that the decreased amount of the active form of PP2A for dephosphorylation of tau may shift the kinase/phosphatase balance to the phosphorylation side.

The present study shows that tau is hyperphosphorylated at multiple sites including Ser202, Ser214, Thr217, Thr231, Ser396, and Ser404 in NPC1-deficient cells. Phosphorylation of tau at sites including Ser202 and Ser396/404, which are the target sites of MAPK, can be explained as a phenomenon promoted by highly activated MAPK (Billingsley and Kincaid 1997), similar to the *in vivo* case (Sawamura *et al.* 2001). However, phosphorylation of other sites cannot be explained in terms of the activated MAPK. In addition, Ser202 and Ser396/404 are known to be the target sites, at which tau could be dephosphorylated by PP2A (Goedert *et al.* 1992a; Drewes *et al.* 1993; Gong *et al.* 1994; Yamamoto *et al.* 1995). This fact indicates that the decreased ability of PP2A may not be able to explain why tau phosphorylation is enhanced at Ser214, Thr217, and Thr231. These lines of evidence, thus, suggest that tau-directed kinases and phosphatases other than MAPK and PP2A may also be involved in the promotion of tau phosphorylation in CT43 cells. Further studies are required in order to identify these tau-directed kinases and phosphatases in NPC1-deficient cells.

There are several possible explanations for the MAPK activation in NPC1-deficient CT43 cells: (i) a decrease in cholesterol level at specific cellular compartments due to a defect in cholesterol trafficking; (ii) the accumulation of cholesterol and other lipids in the lysosomal/late endosomal compartment; or (iii) the direct result of a defect in the NPC1 function. Our findings presented here favor possibility (i) for the following reasons. With respect to the involvement of cholesterol deficiency in the mechanism underlying the promotion of tau phosphorylation in CT43 cells, we found that CT43 cells are more sensitive to amphotericin B than 25RA cells (Fig. 5), suggesting that the cholesterol level in the plasma membrane of CT43 cells is lower than that of 25RA cells. This result is consistent with that of a previous study using NPC-like mutant CHO cells (Dahl *et al.* 1992). Moreover, we have found a more direct evidence, that is the cholesterol level in LDM fraction, which is involved in signal transduction, is clearly reduced (Fig. 6), suggesting that these domain-dependent signal pathways including MAPK pathway are affected in NPC1-deficient cells. This result is supported by a previous findings that cholesterol depletion in the caveolae induces the activation of ERK (Furuchi and Anderson 1998), that ERK is activated in NPC1-deficient human fibroblasts (our unpublished data), and that cholesterol level in DIGs fraction is decreased in NPC1-dificient fibroblasts (Garver *et al.* 2002). Similar results were observed, that is, the cellular cholesterol level of primary neurons was reduced following treatment with compactin, an HMG-CoA reductase inhibitor; the distribution peak of cholesterol in LDM fraction was not observed and MAPK activity was enhanced (Fig. 7). Under these conditions, as we have previously reported, phosphorylation of tau is enhanced (Fan *et al.* 2001). It is widely believed that detergent-insoluble, low-density membrane domains, named raft or DIGs, play critical roles including intracellular signaling pathways (Brown and London 1997; Simons and Ikonen 1997). Therefore it is possible to postulate that alterations in the cholesterol level in LDM domain, whose metabolism is regulated by NPC1-dependent cholesterol trafficking, result in alterations in the activities of kinases/phosphatases including MAPK and PP2A, and in subsequent hyperphosphorylation of tau. However, as a recent study has demonstrated that the NPC1 protein functions as an ATP-dependent permease that belongs to a drug efflux pump superfamily (Davies *et al.* 2000; Ioannou 2001), we may not be able to exclude the possibility that NPC1 participates in other functions, such as cellular signal transduction process(es), in addition to its role in the intracellular cholesterol distribution process.

References

Alessi D. R., Cuenda A., Cohen P., Dudley D. T. and Saltiel A. R. (1995) PD 098059 is a specific inhibitor of the activation of mitogen-activated protein kinase kinase *in vitro* and *in vivo*. *J. Biol. Chem* **270**, 27489–27494.

Auer I. A., Schmidt M. L., Lee V. M., Curry B., Suzuki K., Shin R. W., Pentchev P. G., Carstea E. D. and Trojanowski J. Q. (1995) Paired helical filament tau (PHFtau) in Niemann–Pick type C disease is similar to PHFtau in Alzheimer's disease. *Acta Neuropathol* **90**, 547–551.

Billingsley M. L. and Kincaid R. L. (1997) Regulated phosphorylation and dephosphorylation of tau protein: effects on microtubule interaction, intracellular trafficking and neurodegeneration. *Biochem. J.* **323**, 577–591.

Blanchette-Mackie E. J., Dwyer N. K., Amende L. M., Kruth H. S., Butler J. D., Sokol J., Comly M. E., Vanier M. T., August J. T., Brady R. O. *et al.* (1988) Type-C Niemann–Pick disease: low-density lipoprotein uptake is associated with premature cholesterol accumulation in the Golgi complex and excessive cholesterol storage in lysosomes. *Proc. Natl Acad. Sci. USA* **85**, 8022–8026.

Brown D. A. and London E. (1997) Structure of detergent-resistant membrane domains: does phase separation occur in biological membranes? *Biochem. Biophys. Res. Commun* **240**, 1–7.

Carstea E. D., Morris J. A., Coleman K. G., Loftus S. K., Zhang D., Cummings C., Gu J., Rosenfeld M. A., Pavan W. J., Krizman D. B., Nagle J., Polymeropoulos M. H., Sturley S. L., Ioannou Y. A., Higgins M. E., Comly M., Cooney A., Brown A., Kaneski C. R., Blanchette-Mackie E. J., Dwyer N. K., Neufeld E. B., Chang T. Y., Liscum L., Strauss J. F., IIIOhno K., Zeigler M., Carmi R., Sokol J., Markie D., O'Neill R. R., van Diggelen O. P., Elleder M., Patterson M. C., Brady R. O., Vanier M. T., Pentchev P. G. and Tagle D. A. (1997) Niemann–Pick C1 disease gene: homology to mediators of cholesterol homeostasis. *Science* **277**, 228–231.

Chang T. Y. and Limanek J. S. (1980) Regulation of cytosolic acetoacetyl co-enzyme A thiolase, 3-hydroxy-3- methylglutaryl coenzyme A synthase, 3-hydroxy-3-methylglutaryl co-enzyme A reductase, and mevalonate kinase by low-density lipoprotein and by 25-hydroxycholesterol in Chinese hamster ovary cells. *J. Biol. Chem.* **255**, 7787–7795.

Cruz J. C. and Chang T. Y. (2000) Fate of endogenously synthesized cholesterol in Niemann–Pick type C1 cells. *J. Biol. Chem.* **275**, 41309–40316.

Cruz J. C., Sugii S., YuC. and Chang T. Y. (2000) Role of Niemann–Pick type C1 protein in intracellular trafficking of low-density lipoprotein-derived cholesterol. *J. Biol. Chem.* **275**, 4013–4021.

Dahl N. K., Reed K. L., Daunais M. A., Faust J. R. and Liscum L. (1992) Isolation and characterization of Chinese hamster ovary cells defective in the intracellular metabolism of low-density lipoprotein-derived cholesterol. *J. Biol. Chem.* **267**, 4889–4896.

Davies J. P., Chen F. W. and Ioannou Y. A. (2000) Transmembrane molecular pump activity of Niemann–Pick C1 protein. *Science* **290**, 2295–2298.

Drewes G., Mandelkow E. M., Baumann K., Goris J., Merlevede W. and Mandelkow E. (1993) Dephosphorylation of tau protein and Alzheimer paired helical filaments by calcineurin and phosphatase-2A. *FEBS Lett.* **336**, 425–432.

Dudley D. T., Pang L., Decker S. J., Bridges A. J. and Saltiel A. R. (1995) A synthetic inhibitor of the mitogen-activated protein kinase cascade. *Proc. Natl Acad. Sci. USA* **92**, 7686–7689.

Fan Q. W. YuW., Senda T., Yanagisawa K. and Michikawa M. (2001) Cholesterol-dependent modulation of tau phosphorylation in cultured neurons. *J. Neurochem.* **76**, 391–400.

Fielding P. E. and Fielding C. J. (1995) Plasma membrane caveolae mediate the efflux of cellular free cholesterol. *Biochemistry* **34**, 14288–14292.

Furuchi T. and Anderson R. G. (1998) Cholesterol depletion of caveolae causes hyperactivation of extracellular signal-related kinase (ERK). *J. Biol. Chem.* **273**, 21099–21104.

Garver W. S., Krishnan K., Gallagos J. R., Michikawa M., Francis G. A. and Heidenreich R. A. (2002) Niemann–Pick C1 protein regulates cholesterol transport to the *trans*-Golgi network and plasma membrane caveolae. *J. Lipid Res.* **43**, 579–589.

Goedert M., Cohen E. S., Jakes R. and Cohen P. (1992a) p42 MAP kinase phosphorylation sites in microtubule-associated protein tau are dephosphorylated by protein phosphatase 2A1. Implications for Alzheimer's disease. (published erratum appears in *FEBS Lett.* 1992; **313**, 203). *FEBS Lett.* **312**, 95–99.

Goedert M., Spillantini M. G., Cairns N. J. and Crowther R. A. (1992b) Tau proteins of Alzheimer paired helical filaments: abnormal phosphorylation of all six brain isoforms. *Neuron* **8**, 159–168.

Goedert M., Trojanwski J. Q. and Lee M.-Y. (1996) The Neurofibrillary Pathology of Alzheimer's Disease, in *The Molecular and Genetic Basis of Neurological Disease*, 2nd edn. (Rosenberg R. N., Prusiner S. B., DiMauro S. and Barchi R. L., eds), pp. 613–627. Butterworth-Heinemann, Boston.

Gong C. X., Grundke-Iqbal I. and Iqbal K. (1994) Dephosphorylation of Alzheimer's disease abnormally phosphorylated tau by protein phosphatase 2A. *Neuroscience* **61**, 765–772.

Gong C. X., Lidsky T., Wegiel J., Zuck L., Grundke-Iqbal I. and Iqbal K. (2000) Phosphorylation of microtubule-associated protein tau is regulated by protein phosphatase 2A in mammalian brain. Implications for neurofibrillary degeneration in Alzheimer's disease. *J. Biol. Chem.* **275**, 5535–5544.

Gong J. S., Sawamura N., Zou K., Sakai J., Yanagisawa K. and Michikawa M. (2002) Amyloid β-protein affects cholesterol metabolism in cultured neurons: implications for pivotal role of cholesterol in the amyloid cascade. *J. Neurosci. Res.* **70**, 438–446.

Grundke-Iqbal I., Iqbal K., Quinlan M., Tung Y. C., Zaidi M. S. and Wisniewski H. M. (1986a) Microtubule-associated protein tau. A component of Alzheimer paired helical filaments. *J. Biol. Chem.* **261**, 6084–6089.

Grundke-Iqbal I., Iqbal K., Tung Y. C., Quinlan M., Wisniewski H. M. and Binder L. I. (1986b) Abnormal phosphorylation of the microtubule-associated protein tau (tau) in Alzheimer cytoskeletal pathology. *Proc. Natl Acad. Sci. USA* **83**, 4913–4917.

Hartmann T. (2001) Cholesterol, Aβ and Alzheimer's disease. *Trends Neuorsci.* **24**, S45–S48.

Hua X., Nohturfft A., Goldstein J. L. and Brown M. S. (1996) Sterol resistance in CHO cells traced to point mutation in SREBP cleavage-activating protein. *Cell* **87**, 415–426.

Ioannou Y. A. (2001) Multidrug permeases and subcellular cholesterol transport. *Nat. Rev. Mol. Cell Biol.* **2**, 657–668.

Isobe I., Michikawa M. and Yanagisawa K. (1999) Enhancement of MTT, a tetrazolium salt, exocytosis by amyloid β-protein and chloroquine in cultured rat astrocytes. *Neurosci. Lett.* **266**, 129–132.

Kins S., Crameri A., Evans D. R., Hemmings B. A., Nitsch R. M. and Gotz J. (2001) Reduced protein phosphatase 2a activity induces hyperphosphorylation and altered compartmentalization of tau in transgenic mice. *J. Biol. Chem.* **276**, 38193–38200.

Kobayashi T., Beuchat M. H., Lindsay M., Frias S., Palmiter R. D., Sakuraba H., Parton R. G. and Gruenberg J. (1999) Late endosomal membranes rich in lysobisphosphatidic acid regulate cholesterol transport. *Nat. Cell Biol.* **1**, 113–118.

Kosik K. S., Orecchio L. D., Binder L., Trojanowski J. Q., Lee V. M. and Lee G. (1988) Epitopes that span the tau molecule are shared with paired helical filaments. *Neuron* **1**, 817–825.

Koudinov A. R. and Koudinova N. V. (2001) Essential role for cholesterol in synaptic plasticity and neuronal degeneration. *FASEB J.* **15**, 1858–1860.

Lange Y., Ye J., Rigney M. and Steck T. (2000) Cholesterol movement in Niemann–Pick type C cells and in cells treated with amphiphiles. *J. Biol. Chem.* **275**, 17468–17475.

Lee V. M., Balin B. J., Otvos L. Jr and Trojanowski J. Q. (1991) A68: a major subunit of paired helical filaments and derivatized forms of normal Tau. *Science* **251**, 675–678.

Lisanti M. P., Scherer P. E., Vidugiriene J., Tang Z., Hermanowski-Vosatka A., Tu Y. H., Cook R. F. and Sargiacomo M. (1994) Characterization of caveolin-rich membrane domains isolated from an endothelial-rich source: implications for human disease. *J. Cell Biol.* **126**, 111–126.

Liscum L. and Klansek J. J. (1998) Niemann–Pick disease type C. *Curr. Opin. Lipidol.* **9**, 131–135.

Liscum L., Ruggiero R. M. and Faust J. R. (1989) The intracellular transport of low density lipoprotein-derived cholesterol is defective in Niemann–Pick type C fibroblasts. *J. Cell Biol.* **108**, 1625–1636.

Liu Y., Peterson D. A. and Schubert D. (1998) Amyloid beta peptide alters intracellular vesicle trafficking and cholesterol homeostasis. *Proc. Natl Acad. Sci. USA* **95**, 13266–13271.

Love S., Bridges L. R. and Case C. P. (1995) Neurofibrillary tangles in Niemann–Pick disease type C. *Brain* **118**, 119–129.

Michikawa M. and Yanagisawa K. (1998) Apolipoprotein E4 induces neuronal cell death under conditions of suppressed *de novo* cholesterol synthesis. *J. Neurosci. Res.* **54**, 58–67.

Michikawa M. and Yanagisawa K. (1999) Inhibition of cholesterol production but not of non-sterol isoprenoid products induces neuronal cell death. *J. Neurochem.* **72**, 2278–2285.

Michikawa M., Fan Q. W., Isobe I. and Yanagisawa K. (2000) Apolipoprotein E exhibits isoform-specific promotion of lipid efflux from astrocytes and neurons in culture. *J. Neurochem.* **74**, 1008–1016.

Michikawa M., Gong J. S., Fan Q. W., Sawamura N. and Yanagisawa K. (2001) A novel action of Alzheimer's amyloid β-protein (Aβ): oligomeric Aβ promotes lipid release. *J. Neurosci.* **21**, 7226–7235.

Millard E. E., Srivastava K., Traub L. M., Schaffer J. E. and Ory D. S. (2000) Niemann–Pick type C1 (NPC1) overexpression alters cellular cholesterol homeostasis. *J. Biol. Chem.* **275**, 38445–38451.

Neufeld E. B., Wastney M., Patel S., Suresh S., Cooney A. M., Dwyer N. K., Roff C. F., Ohno K., Morris J. A., Carstea E. D., Incardona J. P., Strauss J. F., 3rd Vanier M. T., Patterson M. C., Brady R. O., Pentchev P. G. and Blanchette-Mackie E. J. (1999) The Niemann–Pick C1 protein resides in a vesicular compartment linked to retrograde transport of multiple lysosomal cargo. *J. Biol. Chem.* **274**, 9627–9635.

Norman A. W., Demel R. A., de Kruyff B. and van Deenen L. L. (1972) Studies on the biological properties of polyene antibiotics. Evidence for the direct interaction of filipin with cholesterol. *J. Biol. Chem.* **247**, 1918–1929.

Nukina N. and Ihara Y. (1986) One of the antigenic determinants of paired helical filaments is related to tau protein. *J. Biochem.* **99**, 1541–1544.

Pentchev P. G., Vanier M. T., Suzuki K. and Patterson M. C. (1995) Niemann–Pick disease, type C: a cellualr cholesterol lipidosis. In: *The Metabolic and Molecular Basis of Inherited Disease* (Scriver C. R., Beaudet A. L., Sly W. S. and Valle D., eds), pp. 2625–2640. McGraw-Hill, New York.

Sawamura N., Morishima-Kawashima M., Waki H., Kobayashi K., Kuramochi T., Frosch M. P., Ding K., Ito M., Kim T. W., Tanzi R. E., Oyama F., Tabira T., Ando S. and Ihara Y. (2000) Mutant presenilin 2 transgenic mice. A large increase in the levels of Aβ42 is presumably associated with the low-density membrane domain that contains decreased levels of glycerophospholipid and sphingomyelin. *J. Biol. Chem.* **275**, 27901–27908.

Sawamura N., Gong J. S., Garver W. S., Heidenreich R. A., Ninomiya H., Ohno K., Yanagisawa K. and Michikawa M. (2001) Site-specific phosphorylation of tau accompanied by activation of mitogen-activated protein kinase (MAPK) in brains of Niemann–Pick type C mice. *J. Biol. Chem.* **276**, 10314–10319.

Simons K. and Ikonen E. (1997) Functional rafts in cell membranes. *Nature* **387**, 569–572.

Simons M., Keller P., Dichgans J. and Schulz J. B. (2001) Cholesterol and Alzheimer's disease: is there a link? *Neurology* **57**, 1089–1093.

Sontag E., Nunbhakdi-Craig V., Lee G., Brandt R., Kamibayashi C., Kuret J., White C. L., 3rd Mumby M. C. and Bloom G. S. (1999) Molecular interactions among protein phosphatase 2A, tau, and microtubules. Implications for the regulation of tau phosphorylation and the development of tauopathies. *J. Biol. Chem.* **274**, 25490–25498.

Suzuki K., Parker C. C., Pentchev P. G., Katz D., Ghetti B., D'Agostino A. N. and Carstea E. D. (1995) Neurofibrillary tangles in Niemann–Pick disease type C. *Acta Neuropathol.* **89**, 227–238.

Underwood K. W., Jacobs N. L., Howley A. and Liscum L. (1998) Evidence for a cholesterol transport pathway from lysosomes to endoplasmic reticulum that is independent of the plasma membrane. *J. Biol. Chem.* **273**, 4266–4274.

Vogelsberg-Ragaglia V., Schuck T., Trojanowski J. Q. and Lee V. M. (2001) PP2A mRNA expression is quantitatively decreased in Alzheimer's disease hippocampus. *Exp. Neurol.* **168**, 402–412.

Wood J. G., Mirra S. S., Pollock N. J. and Binder L. I. (1986) Neurofibrillary tangles of Alzheimer's disease share antigenic determinants with the axonal microtubule-associated protein tau (tau) (published erratum appears in *Proc. Natl Acad. Sci. USA* 1986; **83**, 9773). *Proc. Natl Acad. Sci. USA* **83**, 4040–4043.

Xie C., Turley S. D. and Dietschy J. M. (1999a) Cholesterol accumulation in tissues of the Niemann–Pick type C mouse is determined by the rate of lipoprotein-cholesterol uptake through the coated-pit pathway in each organ. *Proc. Natl Acad. Sci. USA* **96**, 11992–11997.

Xie C., Turley S. D., Pentchev P. G. and Dietschy J. M. (1999b) Cholesterol balance and metabolism in mice with loss of function of Niemann–Pick C protein. *Am. J. Physiol.* **276**, E336–E344.

Yamamoto H., Hasegawa M., Ono T., Tashima K., Ihara Y. and Miyamoto E. (1995) Dephosphorylation of fetal-tau and paired helical filaments-tau by protein phosphatases 1 and 2A and calcineurin. *J. Biochem.* **118**, 1224–1231.

Neuropathology 2003; **23**, 64–74

Workshop

Tissue culture methods to study neurological disorders: Establishment of immortalized Schwann cells from murine disease models

Kazuhiko Watabe,[1] Tsuyoshi Sakamoto,[1] Yoko Kawazoe,[1] Makoto Michikawa,[2] Katsuichi Miyamoto,[3] Takashi Yamamura,[3] Hideyuki Saya[4] and Norie Araki[4]

[1]Department of Molecular Neuropathology, Tokyo Metropolitan Institute for Neuroscience, Fuchu, [3]Department of Immunology, National Institute of Neuroscience, National Center of Neurology and Psychiatry, Kodaira, Tokyo, [2]Department of Dementia Research, National Institute for Longevity Sciences, Obu, Aichi and [4]Department of Tumor Genetics and Biology, Kumamoto University School of Medicine, Kumamoto, Japan

Previously the authors have established spontaneously immortalized cell lines from long-term cultures of normal adult mouse Schwann cells. Establishment of such Schwann cell lines derived from murine disease models may greatly facilitate the studies of the cellular mechanisms of their peripheral nervous system lesions in the relevant diseases. Recently the authors have established immortalized Schwann cell lines derived from Niemann–Pick disease type C mice (NPC; *spm/spm*) and globoid cell leukodystrophy mice (twitcher). In the present study long-term cultures were maintained of Schwann cells derived from dorsal root ganglia and consecutive peripheral nerves of another NPC mice (*npc^{nih}/npc^{nih}*, *npc^{nih}/+*), myelin P0 protein-deficient mice (*P0–/–*, *P0+/–*) with their wild-type littermates (*P0+/+*), and neurofibromatosis type 1 gene (*NF1*)-deficient mice (*Nf1^{Fcr}/+*) for 8–10 months, and immortalized cell lines from all these animals established spontaneously. These cell lines had spindle-shaped Schwann cell morphology and distinct Schwann cell phenotypes and retained genomic and biochemical abnormalities, sufficiently representing the *in vivo* pathological features of the mutant mice. These immortalized Schwann cell lines can be useful in studies of nervous system lesions in these mutant mice and relevant human disorders.

Key words: cell line, myelin P0 protein, neurofibromatosis type 1, Niemann–Pick disease type C, Schwann cell.

Correspondence: Kazuhiko Watabe, MD, PHD, Department of Molecular Neuropathology, Tokyo Metropolitan Institute for Neuroscience, 2-6, Musashidai, Fuchu, Tokyo 183-8526, Japan.
Email: kazwtb@tmin.ac.jp
Received and accepted 1 October 2002.

INTRODUCTION

During development and regeneration of the peripheral nervous system (PNS), Schwann cells are responsible for providing trophic support for the growth and maintenance of neurons and ensheathing their axons in either a myelinating or an unmyelinating form. To investigate regulatory mechanisms of neuron–Schwann cell interactions *in vitro*, many investigators have established immortalized Schwann cell lines.[1–12] In these we have previously obtained adult mouse Schwann cell lines either by transfection of SV40 large T antigen gene (MS1)[5] or by spontaneous immortalization (IMS32).[10] More recently, we have also established and characterized spontaneously immortalized Schwann cells from murine models of Niemann–Pick disease type C (NPC), *spm/spm*,[13] and globoid cell leukodystrophy, twitcher.[14] Establishment of such Schwann cell lines derived from murine disease models may greatly facilitate the studies of the cellular mechanisms of their PNS lesions in the relevant diseases.

In the present study we further characterize the wild-type Schwann cell line IMS32,[10] and describe the establishment of novel Schwann cell lines derived from other murine disease models; that is, other NPC mice (*npc^{nih}/npc^{nih}*, *npc^{nih}/+*), myelin P0 protein-deficient mice (*P0–/–*, *P+/–*) with their wild-type littermates (*P0+/+*), and neurofibromatosis type 1 gene (*NF1*)-deficient mice (*Nf1^{Fcr}/+*).

METHODS

Cell culture

Breeding pairs of the BALB/c heterozygous mice for NPC (*npc^{nih}/+*)[15,16] and C57BL/6 heterozygous *NF1*-deficient